R and D TACOM

LABORATORY

TECHNICAL REPORT

NO. 12622 VOL 1

DESIGN AND FABRICATION OF
FULL SCALE PROTOTYPE TRUCK
CHASSIS (VOLUME 1 - - WHEELS)
JULY 1984

Final Report

CONTRACT NO. DAAK30-79-C-0147

by Frank Y. Soliman
Ewald Associates, Inc.
19450 Fitzpatrick
Detroit, MI 48228

and

Avery H. Fisher
US Army Tank-Automotive Command
ATTN: DRSTA-RSC
Warren, MI 48090

U.S. ARMY TANK-AUTOMOTIVE COMMAND
Warren, Michigan 48090

R and D CENTER

LABORATORY

TECHNICAL REPORT

NO. 12622 VOL. 1

DESIGN AND FABRICATION OF FULL SCALE PROTOTYPE TRUCK CHASSIS (VOLUME 1 - - WHEELS)

JULY 1984

CONTRACT NO. DAAK30-79-C-0147

FRANK Y. SOLIMAN
EWALD ASSOCIATES, INC.
19450 FITZPATRICK
DETROIT, MI 48228

by AND

AVERY H. FISHER
US ARMY TANK-AUTOMOTIVE COMMAND
ATTN: DRSTA-RSC
WARREN, MI 48090

U.S. ARMY TANK-AUTOMOTIVE COMMAND
RESEARCH AND DEVELOPMENT CENTER
Warren, Michigan 48090

NOTICES

This report is not to be construed as an Official Department of the Army position.

Mention of any trade names or manufacturers in this report shall not be construed as an Official indorsement or approval of such product or companies by the U.S. Government.

Destroy this report when it is no longer needed. Do not return it to the originator.

Unclassified

SECURITY CLASSIFICATION OF THIS PAGE *(When Data Entered)*

REPORT DOCUMENTATION PAGE		READ INSTRUCTIONS BEFORE COMPLETING FORM
1. REPORT NUMBER 12622 Vol. 1	2. GOVT ACCESSION NO.	3. RECIPIENT'S CATALOG NUMBER
4. TITLE *(and Subtitle)* Design and Fabrication of Full Scale Prototype Truck Chasis and Wheels Volume 1 - Wheels		5. TYPE OF REPORT & PERIOD COVERED Final Technical Report 6. PERFORMING ORG. REPORT NUMBER
7. AUTHOR(s) Frank Y. Soliman and Avery H. Fisher		8. CONTRACT OR GRANT NUMBER(s) DAAK30-79-C-0147
9. PERFORMING ORGANIZATION NAME AND ADDRESS Ewald Associates, Inc. 19450 Fitzpatrick Detroit, MI		10. PROGRAM ELEMENT, PROJECT, TASK AREA & WORK UNIT NUMBERS IL162601AH91
11. CONTROLLING OFFICE NAME AND ADDRESS DRSTA-RSC US Army Tank-Automotive Command Warren, MI 48090		12. REPORT DATE July 1984 13. NUMBER OF PAGES
14. MONITORING AGENCY NAME & ADDRESS*(if different from Controlling Office)*		15. SECURITY CLASS. *(of this report)* Unclassified 15a. DECLASSIFICATION/DOWNGRADING SCHEDULE

16. DISTRIBUTION STATEMENT *(of this Report)*

Approve for Public Release, Distribution Unlimited.

17. DISTRIBUTION STATEMENT *(of the abstract entered in Block 20, if different from Report)*

18. SUPPLEMENTARY NOTES

19. KEY WORDS *(Continue on reverse side if necessary and identify by block number)*

Composite Materials
Truck Components
Resin Matrix Composites
Wheels
Fiberglass-epoxy

20. ABSTRACT *(Continue on reverse side if necessary and identify by block number)*

The 1100x20 wheel for the M809, M939 truck series was redesigned for structural composites. Finite element analysis of the design was accomplished using material properties developed during this program.

Tooling was designed and manufactured for both the wheel and the lock ring as two independent molds. Composite wheels and lock rings were manufactured using compression molding techniques.

DD FORM 1 JAN 73 1473 EDITION OF 1 NOV 65 IS OBSOLETE

Unclassified

SECURITY CLASSIFICATION OF THIS PAGE *(When Data Entered)*

Laboratory testing was conducted using SAE J267 A procedures and the Indoor Endurance Test of Specification MIL-T-12459D. The composite wheels performed well under the fatigue environment but did not pass the Indoor Endurance Test.

Table of Contents

List of Tables

LIST OF ILLUSTRATIONS

1.0 INTRODUCTION

The U.S. Army Tank-Automotive Command has been interested in improving tactical truck life and performance. This study addressed the problems posed by the M809 and M939 series 5 ton trucks.

Current truck wheels and frames, which are manufactured from conventional materials (primarily steel), exhibit excessive deterioration from corrosion while in service. In order to improve performance in this area and to decrease the overall weight of the vehicle, a few components were selected for conversion to structural composites. This program involves the conversion of a truck wheel from steel to structural composite and the evaluation of these new wheels in the military environment.

Ewald Associates, Inc. considered the most significant variables in the redesign of the current wheels from steel to structural composite materials. These materials have an organic chemical matrix, such as epoxy or vinylester, into which reinforcing fibers such as glass, graphite or aramid are disposed. By proper combination of fibers and matrix, composite wheels can be manufactured to withstand the severe environment in which military vehicles operate. The developed composite wheel proved to be much lighter than its steel counterpart, just as strong if not stronger, more corrosion resistant, and can be manufactured using existing process techniques with some modification for product quality control.

Structural composites, however, are anisotropic in their properties, thus their design requires more complex procedures. These procedures require the use of sophisticated computer programs and are usually based on finite element analysis techniques.

In addition to design and material selection, manufacturing methods must be analyzed and proper measures taken to ensure strict quality controls to achieve the strength, stiffness, toughness and durability required in the part selected.

2.0 WHEEL DESIGN AND ENGINEERING

2.1 Wheel Design

The design of the composite wheel was based on compression molding as the manufacturing process. Both the basic wheel and the retaining ring were to be manufactured using this method.

The initial wheel design, in addition to being thicker in cross-section, employed metal inserts in the mounting holes to withstand the bolt torque. This design was retained until testing showed that a metal retaining ring was required instead of metal inserts.

The wheel assembly was designed to maintain the overall size of the current steel part. The following constraints were used in this design:

2.1.1. Ten equally spaced mounting holes 1.210 to 1.220 inches (30.734 to 30.988 mm) in diameter were molded into the wheel.

2.1.2. The disc and wheel rim were fabricated as an integral assembly. Thus, no rivets were necessary for attaching the two components as is the case with the current steel wheel. A schematic of the developed composite wheel is shown in Figure 1.

2.1.3. Variable thickness cross sections were used to minimize stress concentrations at critical load carrying sections and to allow for a uniform fiber flow during the molding process.

2.1.4. The wheel rim was within all of the Army requirements, i.e. the maximum out of round and the maximum out of flat are both less than 1/16 inch (1.5875 mm).

2.2 Design Approach

The following design approach was followed during the course of the program:

2.2.1. Basic characteristics of the current steel wheel were determined from field data, data supplied by TACOM, and geometric measurments taken from the existing fleet.

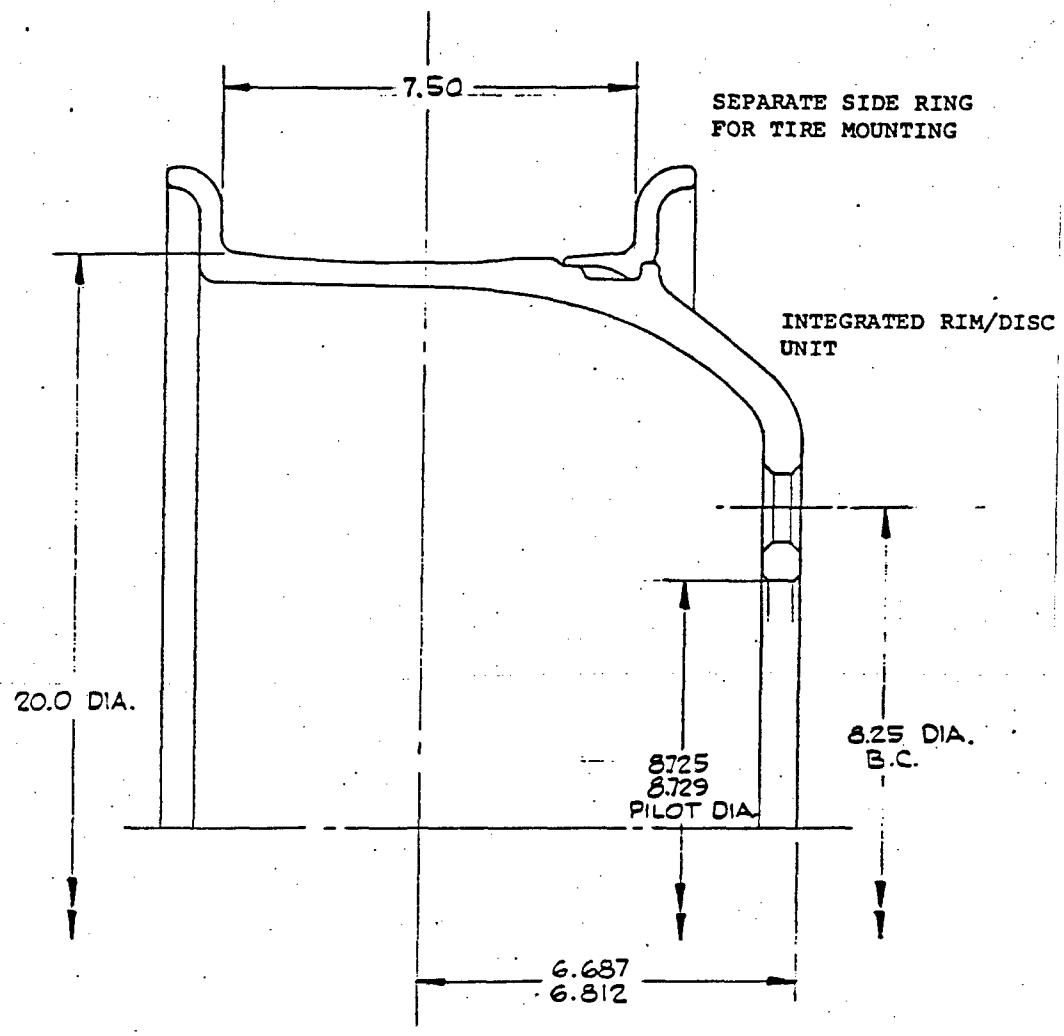

Figure 1 Composite Wheel Assembly (20 x 7.5 In. Wheel)

2.2.2. The input loads on each wheel were evaluated based on the Society of Automotive Engineering (SAE) recommended practices.

2.2.3. Based on load data generated for the steel wheel, various composite wheel designs were investigated. The composite wheel design was based on a symmetrically variable cross-section. This concept aids in minimizing stress concentrations at critical load carrying sections.

2.2.4. A computer model was developed as an aid in the initial stages of the conceptual designs. This is discussed at a later point in this report.

2.2.5. After several initial designs were completed, a complete finite element program was developed and used to determine stress contours in the selected design of the composite plastic wheel under the applied loads supplied by TACOM.

2.2.6. The optimum composite material for the wheel application was introduced in the analysis.

2.2.7. Computer output of the various stress contours in every composite lamina were plotted using the NISA program. Details of the analysis are discussed in section 5.

2.2.8. Readjustment of the wheel thickness was made, based on the computer output and the failure criterion for selected composite laminates. The analysis used the maximum stress theory as the failure criterion. Any local area of high stresses was increased in thickness to allow for a safety factor of at least two.

2.3 Wheel Concept

This concept of variable thickness resulted in a functional composite wheel with minimum weight. This is in contrast to stamped metal wheels where the rim and disk are fabricated by stamping steel sheets of specified thickness.

3.0. DESIGN REQUIREMENTS

The composite wheel design was dictated by the applied loads encountered during the service life of the truck. These loads are numerous and were thoroughly investigated. Some of the load requirements are discussed below.

3.1 Input Loads

The input loads for the wheel design were based on data established by Army specifications and SAE recommended practice. These loads can be classified according to the following requirements the wheel must be able to meet during the truck service life.

3.1.1. Dynamic Cornering Fatigue Test (Figure 2).

The applied force and moment on the wheel were defined as:

$$M = \frac{L[(slr)u=d]}{12} \qquad F = \frac{M}{\text{Moment Arm}}$$

F = Force (lbs)

Where M = Bending moment as applied on the truck wheel (lbs-ft)

L = Load rating of the wheel as specified by Army requirements (LB force) = 5190 LB (2354.2 Kg or 23086 Newton)

slr = Static load radius of the tire to be used on the wheel as specififed by the army (inches) = 20.3 IN (515.62 mm)

u = Coefficient of friction developed between tire and road (=0.70)

d = Offset of wheel = 3.75 inches (95.25 mm)

K = Nondimensional parameter (1.10 to 1.33) = 1.33

The wheel was designed to survive at least 500,000 cycles under these loads without failure.

The wheel should be able to sustain these loads for this number of cycles without the developing cracks that propagate through any of the wheel sections.

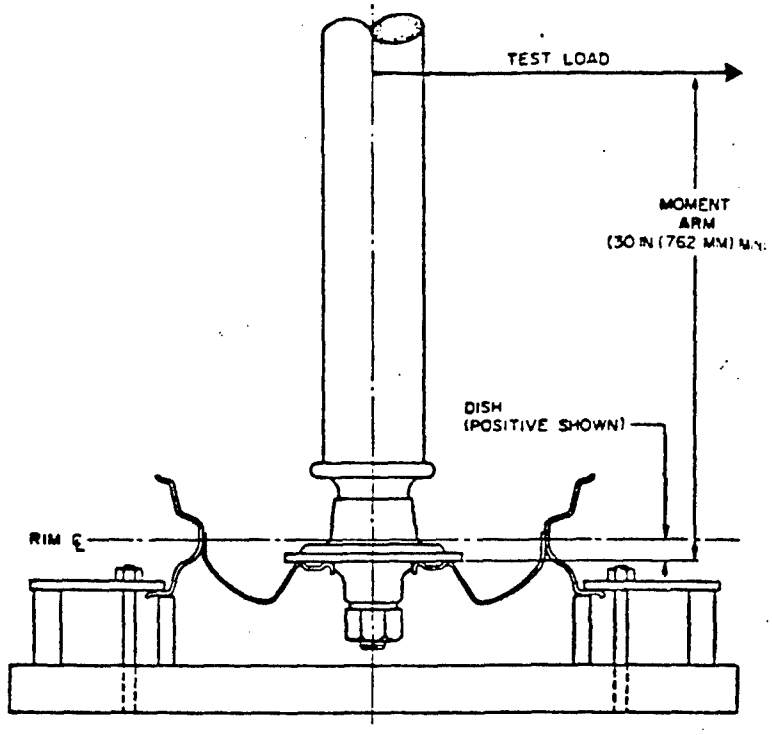

Figure 2 Application of Load During Cornering Fatigue Tests

3.1.2. Rim Dynamic Radial Fatigue Test (Figure 3). The radial load applied to the wheel was determined as follows:

$$F_r = LK$$

Where F_r = Radial force (LB force)

L = Load rating of the wheel as specified by the Army = 5190 pounds.

K = Nondimensional parameter (=2.0)

3.2 Minimum Design cycle life

The mimimum design cycle life for the fabricated composite wheel was 60,000 cycles.

Based on the above requirements, the various composite wheel design concepts were reduced to one optimum design. In this concept the wheel cross-sections remained symmetric. This is the basic cross-section shown in Figure 1. The variables in each concept were primarily wall thickness, distribution of reinforcing ribs, and the number of ribs. During this phase of the development, these parameters were varied to produce a wheel of minimum weight which would withstand the loads imposed during service.

4.0 FINAL DESIGN CONCEPT

The final design concept for the composite wheel is shown in Figure 4. The average wall thickness is approximately 0.75 INCHES (19 mm). Reinforcing ribs (20 ribs at equal intervals around the circumference) were added to provide a uniform load carrying capacity at minimum weight.

4.1 External Dimensions

The external dimensions of the composite wheel were dictated by tire size, location of mounting bolts, and rim diameter. The build up in the plastic wheel thickness was accommodated on the inside of the wheel as shown in Figure 4. No sharp corners between the rim and the disc were permitted. This will allow a gradual transition of the stresses from the disc to the rim, thus eliminating areas of stress concentration and probable initiation of cracks.

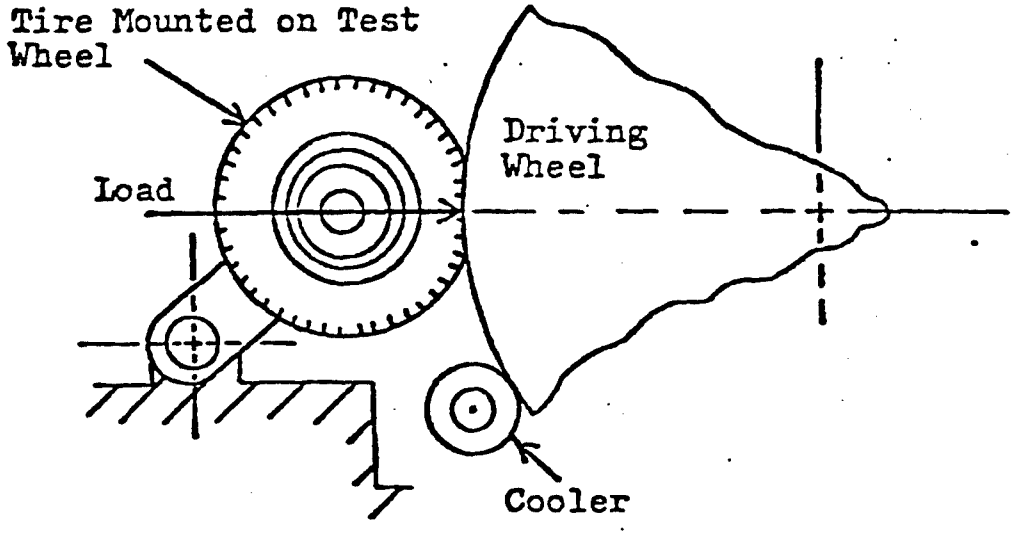

Figure 3 Applied Loads on Wheel During Rim Radial Fatigue Testing

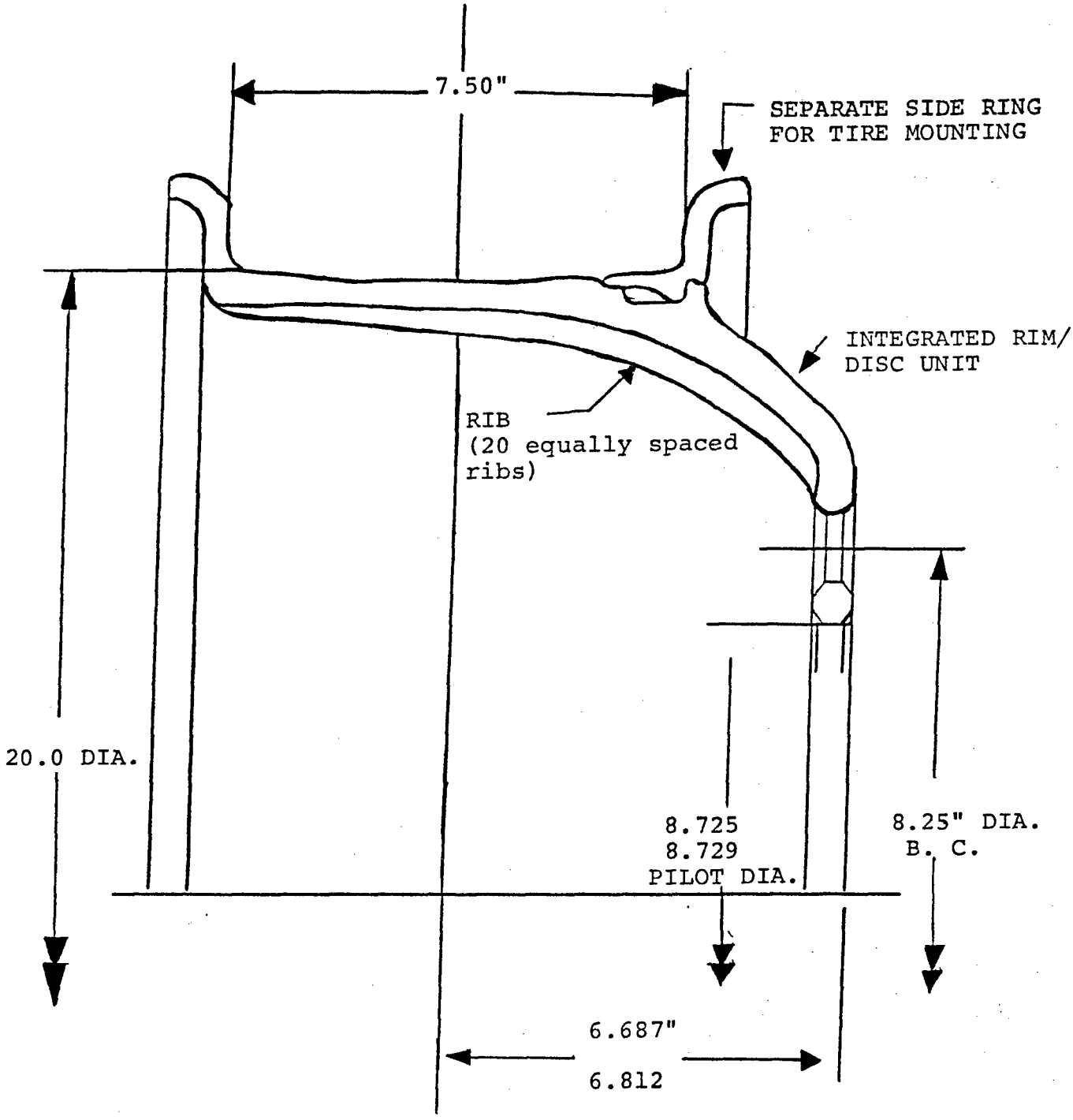

Figure 4

Composite Wheel - Final Design

Areas around the mounting bolts in the disc were formed from thicker material to form bosses. These bosses were reinforced with steel inserts to accept the mounting bolts. This approach was intended to decrease the stresses at the bolt mounting holes and thus avoid enlarging the mounting holes or creating hair line cracks while in service.

4.1.2 The composite wheel design contains ten (10) mounting holes as required in the basic drawing. At first, the wheel was designed with steel inserts to provide the necessary surface for holding the bolts and retaining the necessary torque. Later tests showed that with these inserts there was insufficient material to keep the wheel from cracking. The final design uses a metal ring to provide the necessary surface area to distribute the mounting bolt load adequately.

4.1.3 The composite wheel contains a slot three inches long by 0.26 inches wide (76.2 x 6.604 mm) to provide an opening for the valve stem. In addition, there is a 1/2 inch (12.7 mm) hole in the dish portion of the wheel to allow the valve stem to extend through for servicing.

4.1.4 The resulting truck wheel is corrosion resistant with better geometrical uniformity and a significantly reduced weight. A 50% weight reduction was achieved in the composite wheel as compared to the steel wheel. Because a wheel is an unsprung and rotating mass, this weight reduction is particularly significant with regard to truck ride, vibration, and acceleration.

4.2 Integral disc/rim assembly

4.2.1 The wheel was designed as an integral disc/rim assembly with a separate side ring. The latter was designed as a split composite side locking ring with a 0.092"-0.31" (2.38 to 7.94 mm) gap and breaking slots to complement the composite wheel. This ring is essential for mounting and removal of the tire. The ring also provides sufficient spring force to hold the tire in place while the wheel is in service.

4.2.2 Details of the split-in ring with the breaking slot are shown in Figure 5. It should be noted that the details of the breaking slot and the split-in are identical to those used in the current steel side ring. The prime difference is is that this ring was fabricated from continuous fiber reinforced composite material.

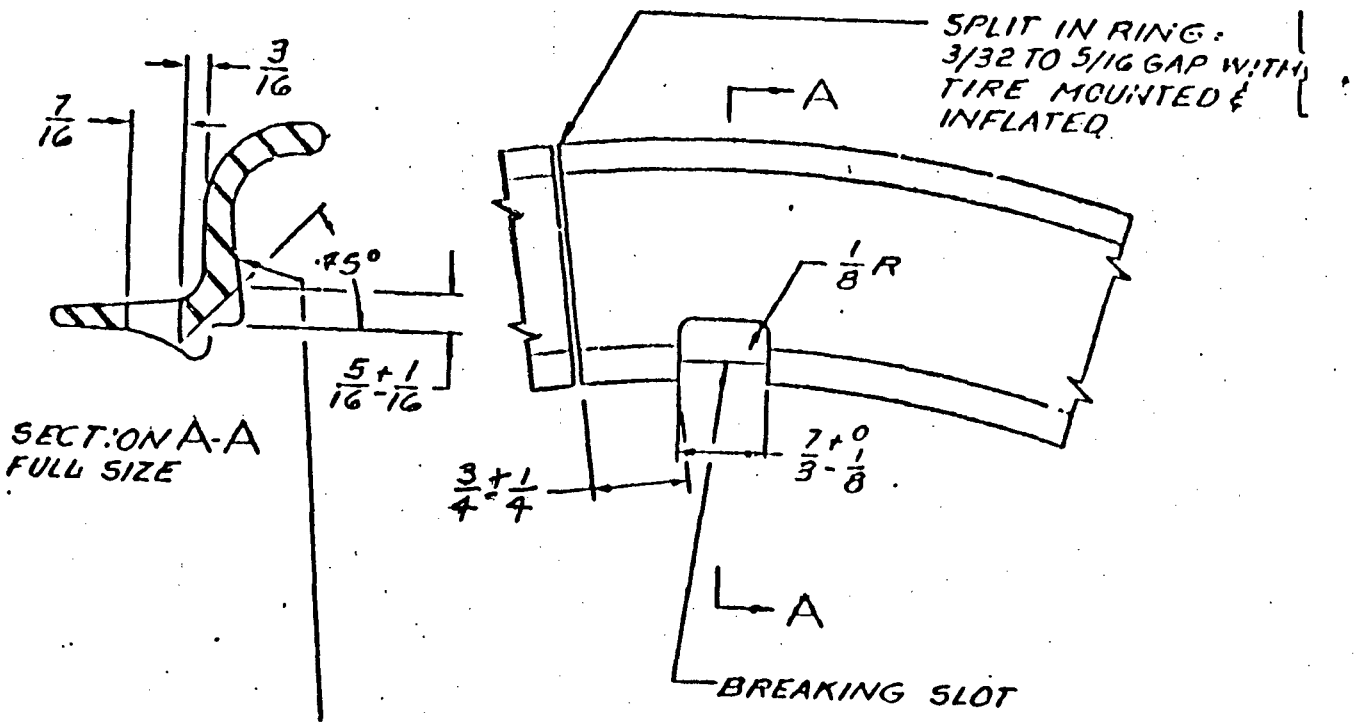

Figure 5 Details of the Hybrid Composite Side Ring

4.2.3 A view of the assembled disc/rim composite part, the associated side ring, and a mounted tire is shown in Figure 6.

5.0 ENGINEERING ANALYSIS

The basic design of the wheel was completed and optimized. The wheel was anaylzed using finite element modeling. The NISA computer model was used in conjunction with thick shell elements to present the wheel structure. Three dimensional (Instead of two dimensional) elements were employed, to accurately duplicate the geometric features of the composite wheel design. Because this design is symmetric, only half of the wheel was modeled. The concentrated stresses around the mounting holes were analyzed separately. The wheel ring was also modeled independently. Use of common nodes between the ring and the wheel provided displacement continuity, and common stresses provided an accurate and realistic simulation of the actual structure.

5.1 Computer Analysis

Computer analysis of the plastic wheel under the aforementioned loading conditions were used. The resulting stresses between the disc/rim joining area, between the assembly and the attached side ring, and around the mounting holes, were determined. These are the most critical areas, since they are exposed to high stresses. High stress concentrations occur around the mounting holes, where the truck weight is transmitted via the mounting bolts.

5.2.1 Since the composite wheel is far from a duplication of the current steel wheel, a detailed finite element analysis was conducted. The analysis was based on the following:

5.2.1.1 Proper composite material allowables based on a 35 percent confidence level.

5.2.1.2 A fine mesh grid system using a two dimensional shell element for each composite layer of the wheel section.

5.2.1.3 A specially adoptable computer program (NISA) designed for laminated composite materials was used. This program uses finite shell elements to model the wheel.

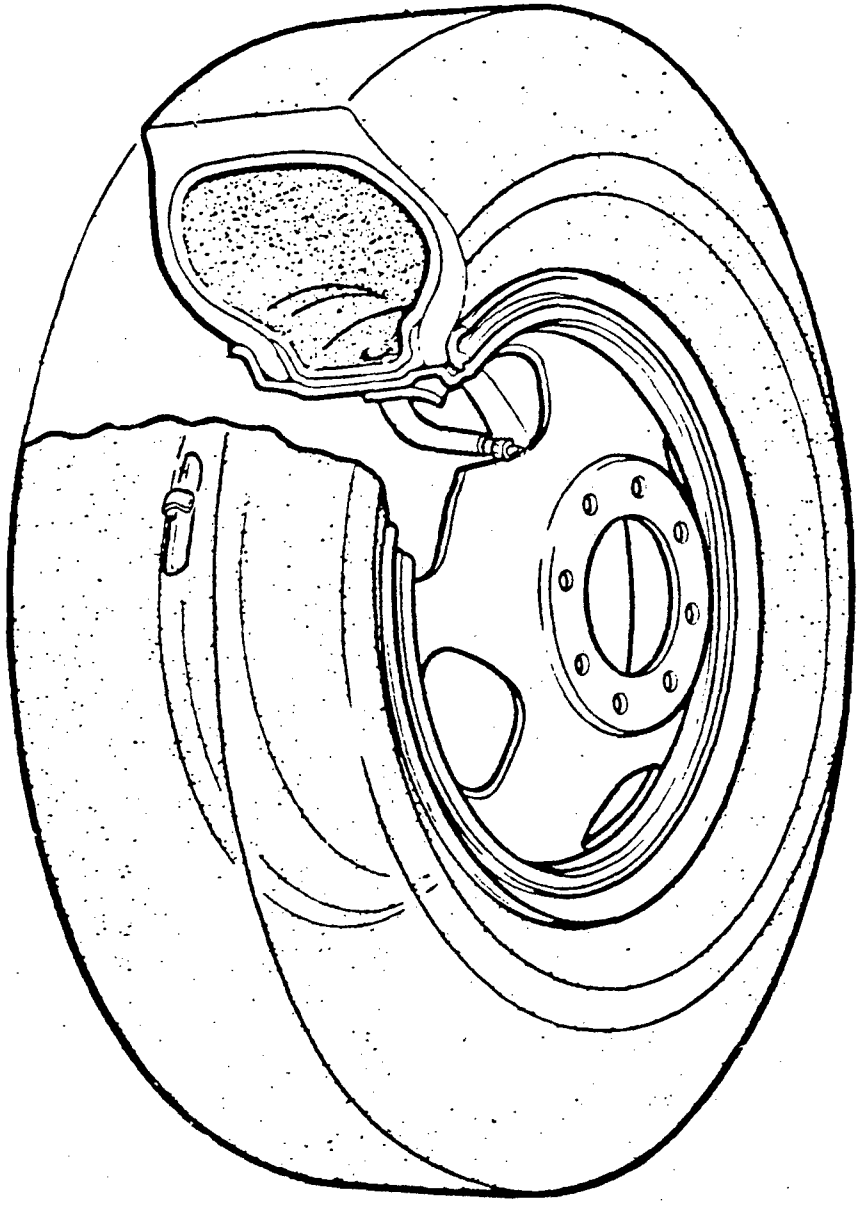

Figure 6 Assembled Composite Wheel with Tire Mounted

(Conceptual Design)

5.2.1.4 Since the wheel was fabricated from oriented composite materials, the material anisotropy and bending-extensional coupling will be necessary features in the analysis.

5.2.1.5 The use of shell elements (tailored for composite materials) for modeling the wheel structure. These elements included the following parameters:

5.2.1.5.1 The effect of transverse shear deformation and rotary inertia

5.2.1.5.2 Material anisotropy

5.2.1.5.3 Bending/extensional coupling due to fiber orientation

5.2.1.5.4 Other material characteristics

5.3 Finite Element Presentation of the Composite Wheel

5.3.1 Various size finite shell elements were used in this analysis. Very small size elements were used around the mounting holes, at the rim/disc intersection, and at the side ring attachment areas. This allowed the detection of any high stress concentration, especially around the mounting bolts.

5.3.2 A typical finite element model of the composite wheel is shown in Figure 7. Due to structural and load symmetry, only one quarter of the wheel structure was modeled. Figure 8 dipicts a model of the truck wheel with computer-generated plots of stress contours.

5.3.3 To calculate the ultimate stresses of each lamina, the overall properties of the lamina were determined using engineering constants for an orthotropic material. Fiber orientation and basic properties of each lamina were based on developed experimental data. The contribution of each lamina to the overall laminate properties is a function of lamina thickness relative to overall laminate thickness. The effect of fiber orientation in each lamina on the engineering constants was determined by mathematical transformations based on the angle between the fibers and the global coordinates of the structure under investigation. This coordinate relationship is shown in Figure 9.

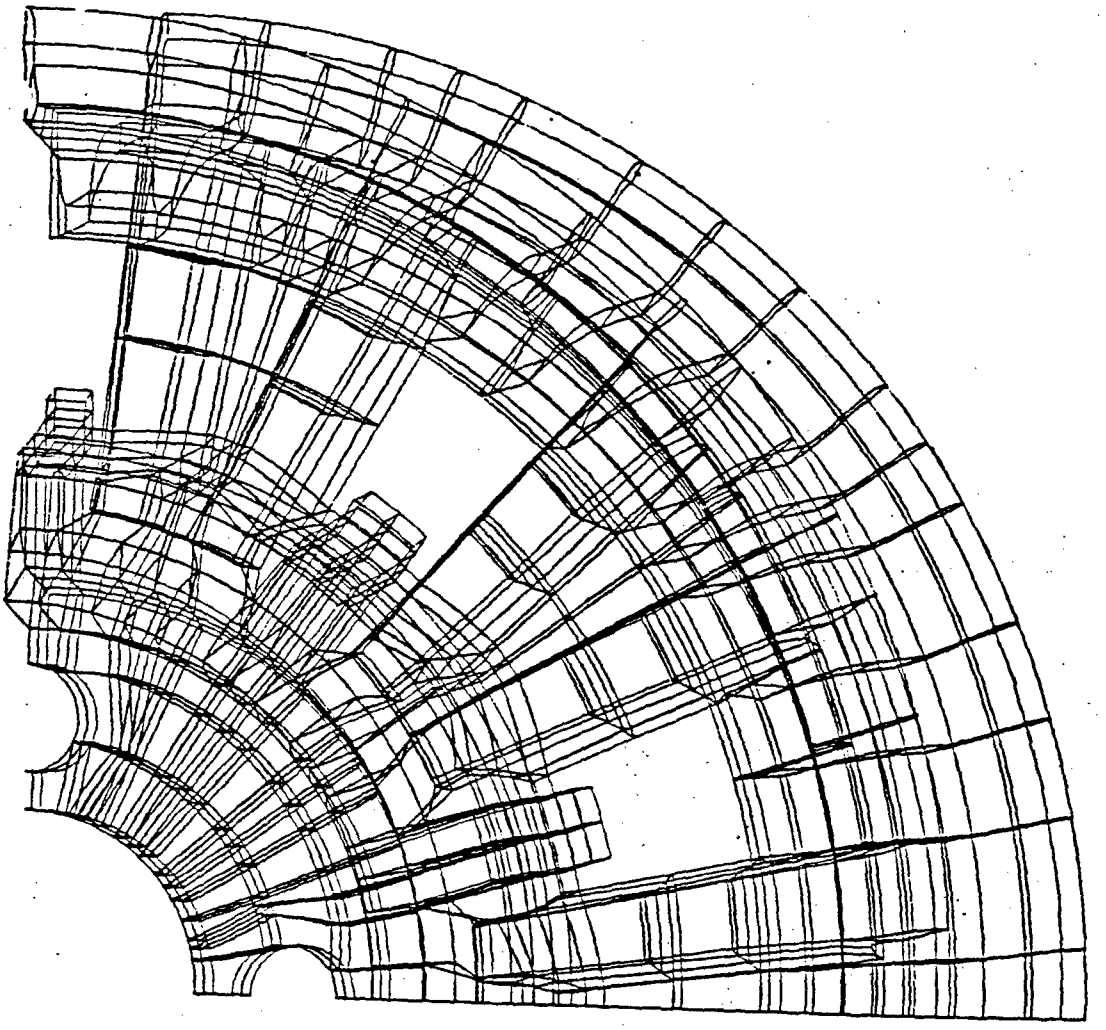

Figure 7 Typical Element Model of a Classic Wheel

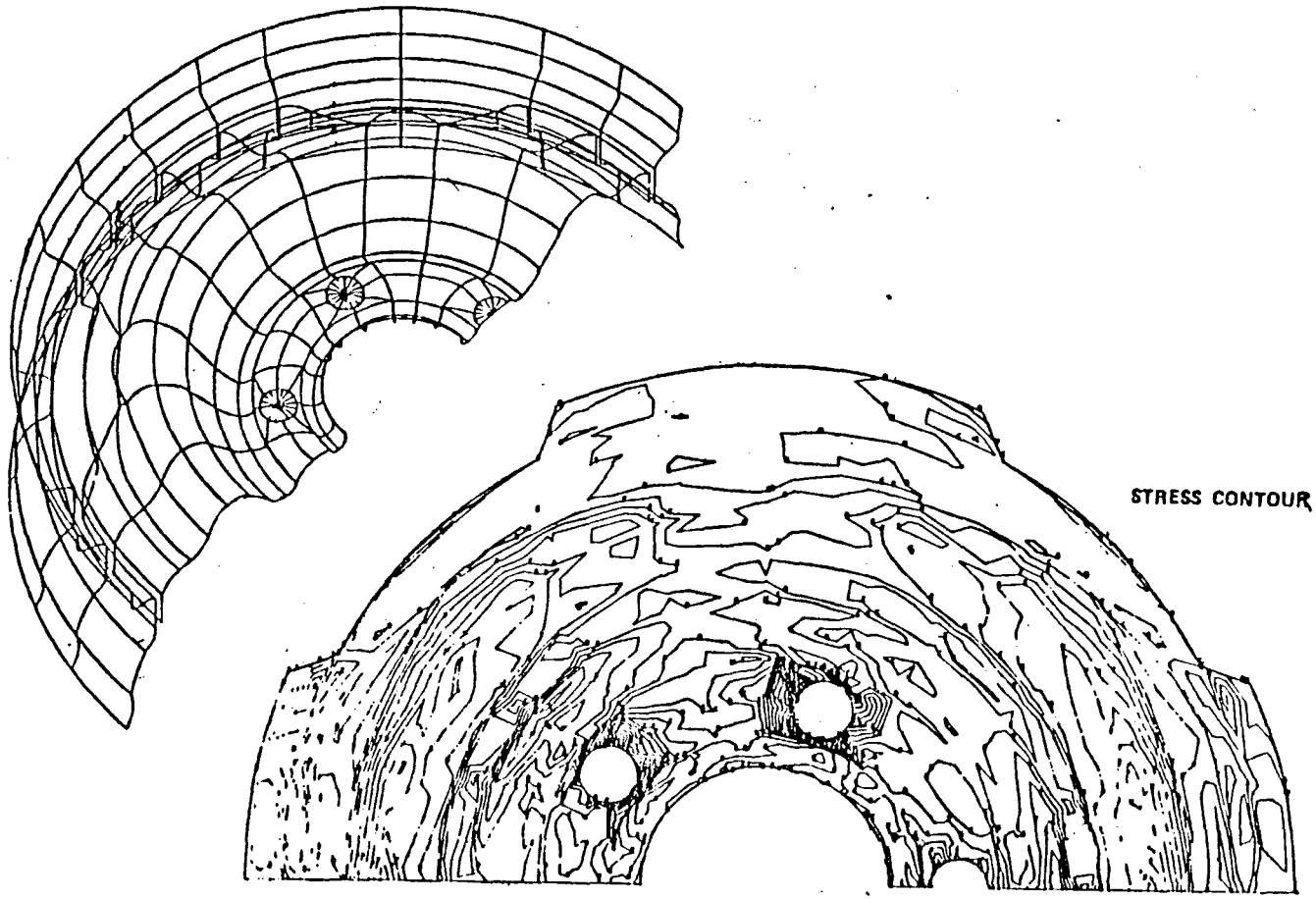

FIGURE 8 **NISA – FINITE ELEMENT MODEL**
OF A WHEEL AND STRESS CONTOUR OUTPUT

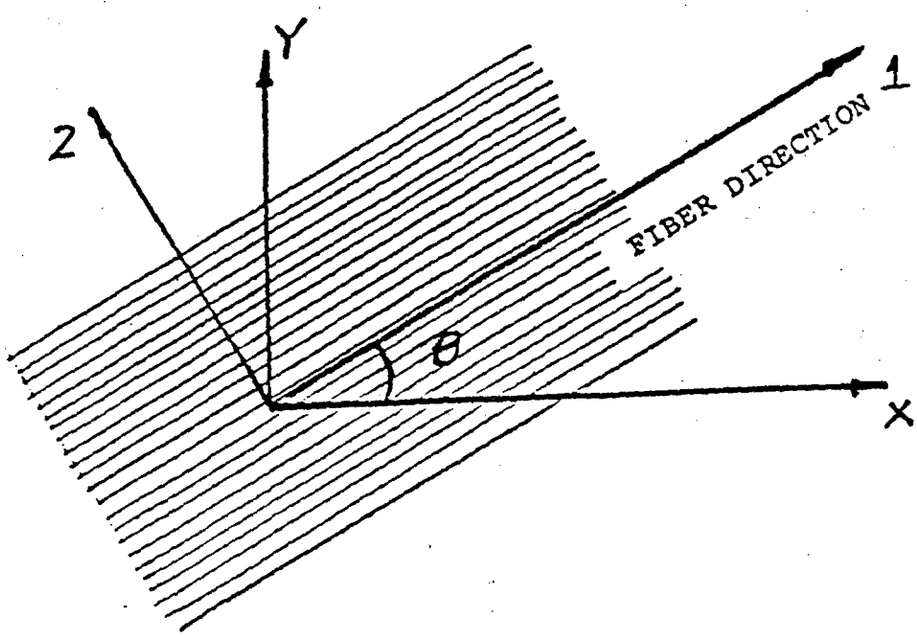

Figure 9 Fiber Directions with Respect to Global Axis X,Y of Structural Components.

Thus, for a lamina with fibers orientated at an angle O with respect to the global x axis of the structure, the following expressions for the lamina modulus can be obtained:

$$\frac{1}{E_{xx}} = \frac{1}{E_{11}} \cos^4\theta + \left(\frac{1}{G_{12}} - \frac{2u_{12}}{E_1}\right) \sin^2\theta \cos^2\theta + \frac{1}{E_{22}} \sin^4\theta$$

$$\frac{1}{E_{yy}} = \frac{1}{E_{22}} \cos^4\theta + \left(\frac{1}{G_{21}} - \frac{2u_{21}}{E_2}\right) \sin^2\theta \cos^2\theta + \frac{1}{E_{11}} \sin^4\theta$$

5.3.4 It was assumed that the strain of each orthotropic lamina is within the linear range of Hook's law, and the stresses and strains were treated as second rank tensors.

The transformation of the stresses/strains from one set of axis to another for each lamina were derived from the equilibrium of a small element as shown in Figure 10.

5.3.5 Assuming a biaxial state of stresses, one can obtain the following relationships:

$$\sigma_{11} = \sigma_{xx} (\cos^2\theta) + \sigma_{yy} (\sin^2\theta) + \tau_{xy} (2 \sin\theta \cos\theta)$$

$$\sigma_{22} = \sigma_{xx} (\sin^2\theta) + \sigma_{yy} (\cos^2\theta) - \tau_{xy} (2 \sin\theta \cos\theta)$$

$$\tau_{12} = -\sigma_{xx} (\sin\theta \cos\theta) + \sigma_{yy} (\sin\theta \cos\theta) + \tau_{xy} (\cos^2\theta - \sin^2\theta)$$

Similarly, the strains in each lamina can be expressed as:

$$\epsilon_{11} = \epsilon_{xx} (\cos^2\theta) + \epsilon_{yy} (\sin^2\theta) + \gamma_{xy} (\sin\theta \cos\theta)$$

$$\epsilon_{22} = \epsilon_{xx} (\sin^2\theta) + \epsilon_{yy} (\cos^2\theta) - -\gamma_{xy} (\sin\theta \cos\theta)$$

$$\gamma_{xy} = -2\epsilon_{xx} (\sin\theta \cos 0) + 2\epsilon_{yy} (\sin 0 \cos 0) + \gamma_{xy} (\cos^2 0 - \sin^2 0)$$

Where:

ϵ_{11} and σ_{11} are the lamina stress and strain along the fiber direction (11).

ϵ_{22} and σ_{22} are the lamina stress and strains perpendicular to the fiber direction.

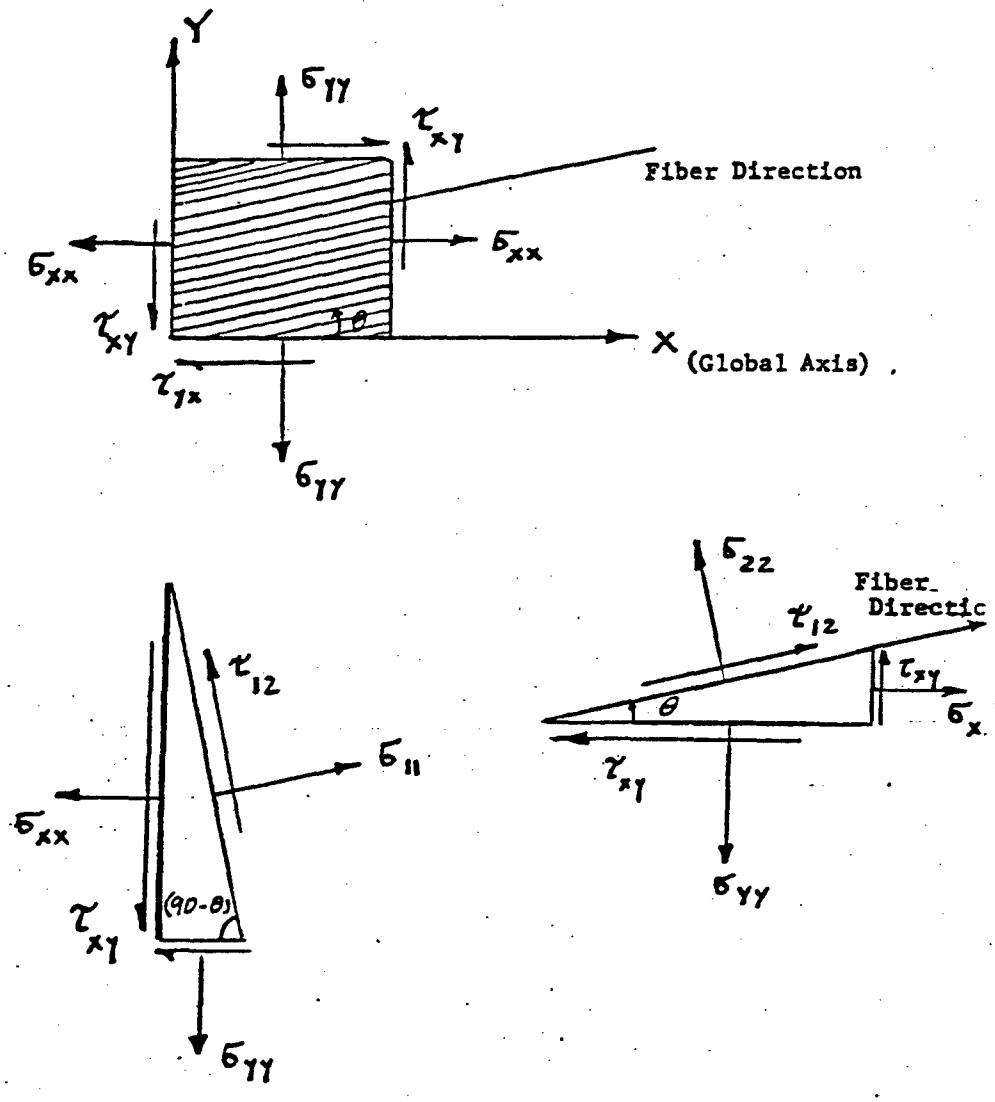

Figure 10 Orthotropic Lamina Under Biaxial Stresses

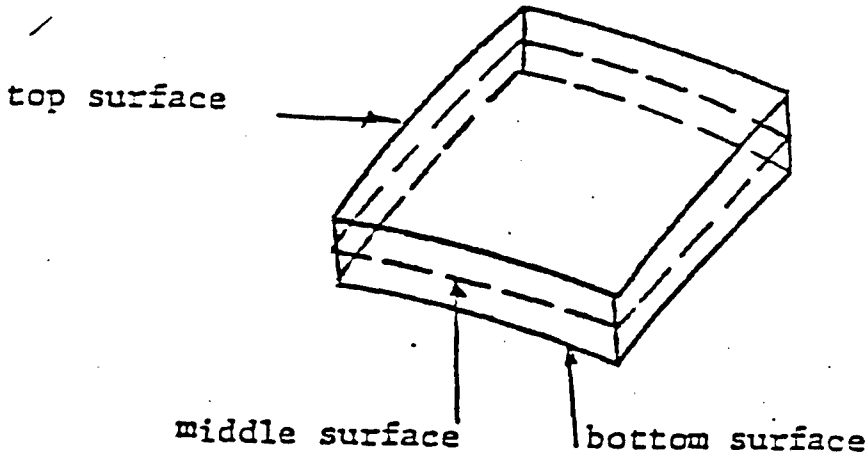

Figure 11 Eight Node Isoparametric General Shell Finite Element

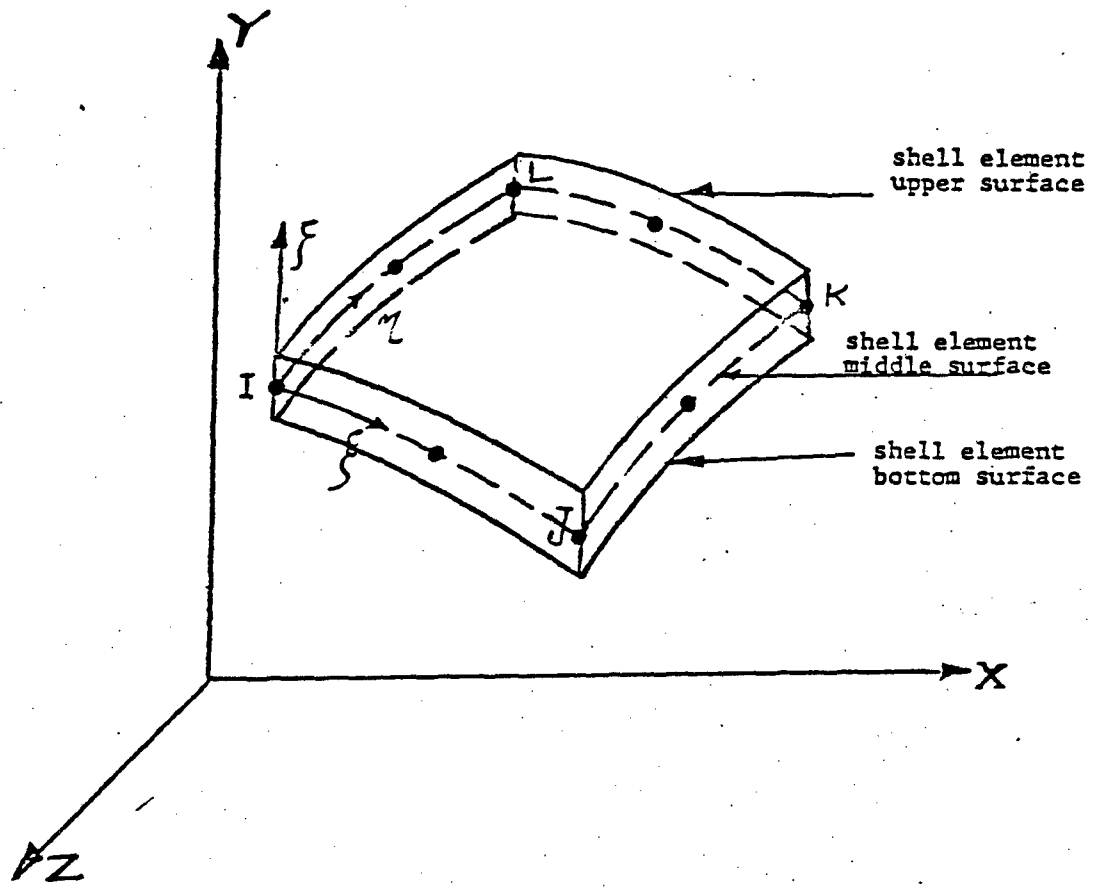

X, Y, Z	global cartesian coordinate system of the structure
ξ, ζ, η	shell element local coordinate system
I, J, K, L	element corner nodal points

Figure 12 General Shell Element and Various Coordinate Systems

t_{12} and ϵ_{12} are the shear stress and strains of the lamina.

θ = angle of orientation of the lamina with respect to the global axis of the structure.

Solving the above relations, one can obtain the lamina properties in the global axis system as a function of lamina orientation. Based on these relationships the ultimate elastic strength for each lamina can be expressed.

5.3.6 A numerically integrated finite element program was used to evaluate the stresses and strains in each composite lamina, as well as the overall deformation of the composite wheel.

5.3.6.1 The computer program is basically designed for laminated composite structural systems. The elements are eight node isoparametric general shell finite elements as shown in Figure 11. Each shell node has its own local coordinate system, which is defined and related to the overall global cartesian coordinate system to the wheel. Definitions of these coordinate systems are shown in Figure 12. Each finite element was represented by the middle surface of the shell and was assigned five basic degrees of freedom as shown in Figure 13.

5.4 Computer Programs Used in this Analysis:

The following computer programs were used for the execution of this project:

5.4.1.0 NISA :Overall finite element analysis program

5.4.1.1 NISACHN :To locate coincident local normals for general shell isoparametric elements

5.4.1.2 NISAWFR :To check maximum wavefromt

5.4.1.3 NISAMPG :To generate the coordinates of middle nodes

5.4.1.4 NISAICE :To check input data and to compute element distortion

5.4.1.5 DISPLAY :An interactive isoparametric finite element graphics program

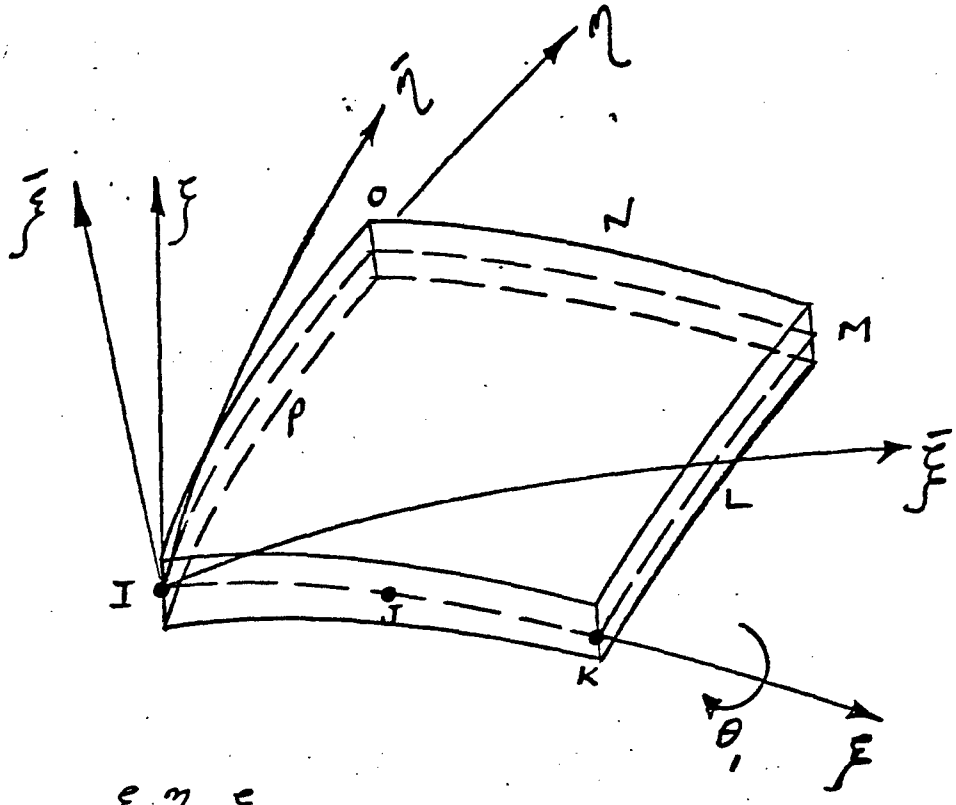

ξ, η, ζ Local Node Coordinate System

$\bar{\xi}, \bar{\eta}, \bar{\zeta}$ Layer Local Coordinate System

Degree of freedom of each node

u_x, u_y, u_z displacements of node in global cartesian coordinate system x, y, z

θ_1, θ_2 rotations about axes of node I respectively

ϕ = angle between principel fiber direction and local element coordinate system

Figure 13 Degrees of Freedom of Shell Element Node Points

5.4.1.6 DIGIT :To digitize geometrical data scaled from the drawing

5.4.1.7 Figures 14 and 15 illustrate the above.

5.5 Computer Output

For each of the load cases analyzed in this investigation, the output from the computer program included the following:

5.5.1.0 A list of all input data

5.5.1.1 Strain energy for each element

5.5.1.2 Reaction forces at each node

5.5.1.3 Nodal displacement

5.5.1.4 Element gauss

5.5.1.5 Stresses computed and printed for principle material directions, i.e., parallel to and normal to the fiber direction. These stresses are:

S_{xx} stress in fiber direction

S_{yy} stress normal to fibers

S_{xy} inplane shear stress

5.5.1.6 Element stress resultants

5.5.1.7 Nodal averaged stress resultants

6.0 MATERIALS

6.1 Discussion

Automotive truck wheels are complex structures subjected to severe loads during service. In steel with a modulus of 30×10^6 psi (206.8 GPa) in all directions, the only properties that need be considered are the tensile strength and fatigue limits. In structural composites,however, the modulus of the material is lower but, its strength may be tailored as a function of material thickness, fiber orientation, and several other parameters.

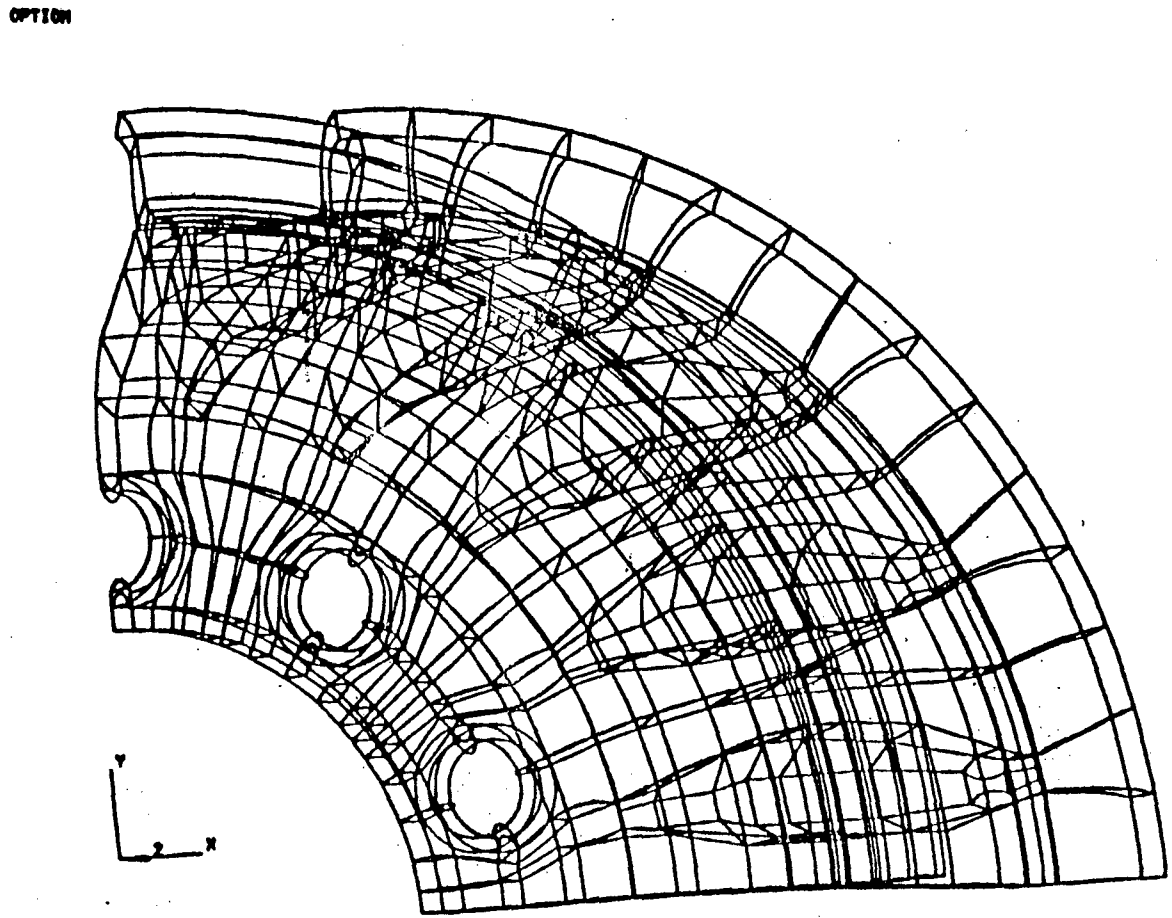

Figure 14 Front View of the Composite Wheel Model, with Mounting Holes

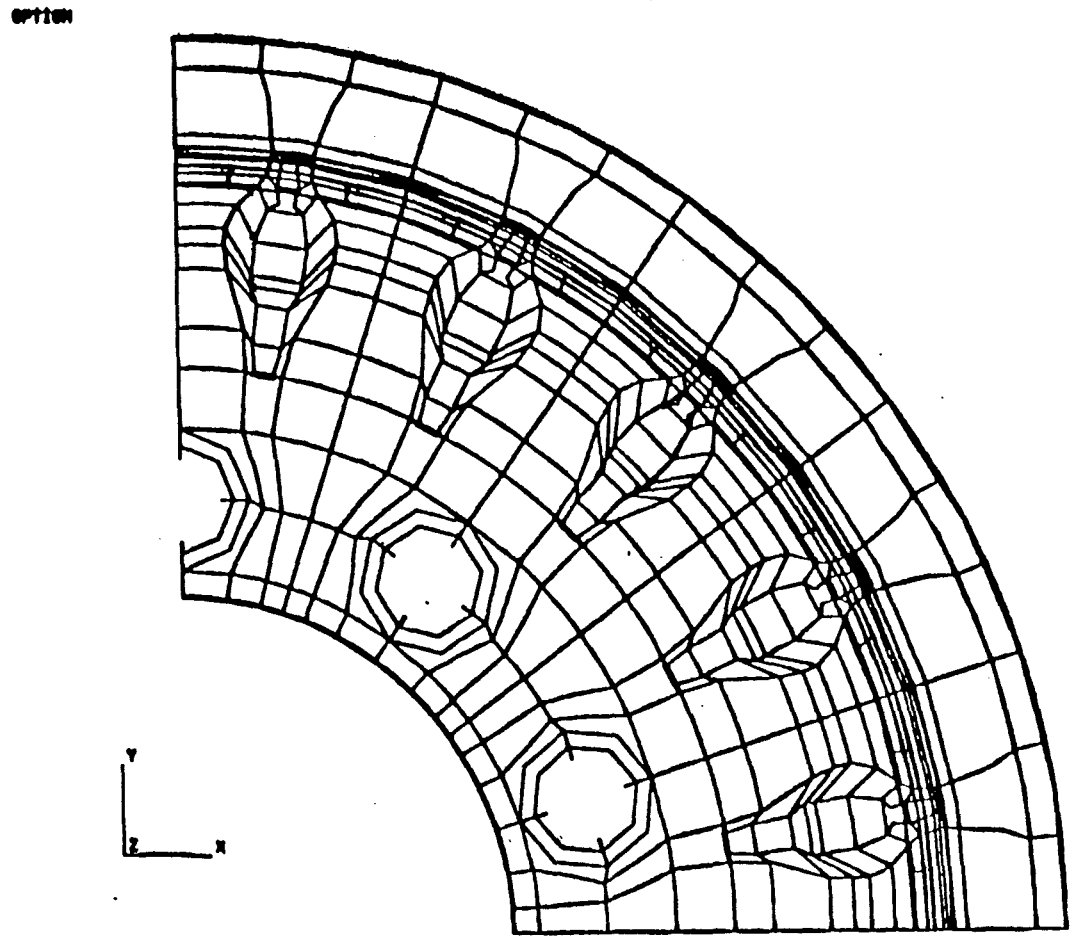

Figure 15 Front View of the Composite Wheel Structure

6.1.2 It was realized that the material to replace the basic steel wheel will be much thicker. In order to determine the exact arrangement of constituent materials, several thick composite plaques (12" x 12" x 1") were molded and cut into test samples for experimental mechanical property determination.

At first a hybrid of glass and graphite composite plies with a resin system of either epoxy or vinylester was considered. However the hybrid system did not provide the neccessary strength.

6.1.3 Many other materials were evaluated using chopped glass in an epoxy resin (similar in nature to SMC compounds in epoxy system). The final material choice called for oriented continuous glass fibers. The fibers were oriented both circumferentially and radially. The basic properties of the constituent materials to be used in the construction have been developed both experimentally and theoretically.

6.2 Material Form

The wheel assembly was fabricated using two materials.

6.2.1 Continuous unidirectional glass sheets (XMC type material)

6.2.2 A chopped glass fiber compound (HMC type material) with high glass loading (65% by weight)

The continuous glass fibers provide the added fatigue strength needed for the wheel environment. The discontinuous fibers aided in the formation of variable wall thickness at various sections of the wheel.

6.3 Compound

A compound of oriented continuous glass fibers and discontinuous glass fibers in a vinylester matrix was utilzed in this application. The compound was supplied in a sheet form with the proper thickness.

6.4 Mechanical Properties

Basic mechanical properties of the discontinous glass compound are shown in Table 1. The properties of the continuous glass compound are shown in Table 2.

TABLE #1

Mechanical Properties of Discontinuous Randomly Oriented E-Glass in Vinylester Resins (Isotropic Laminate)

Properties	Units	Measured Data
Material Density	gm/cc	1.84
Fiber Content (by vol.)	%	45
Tensile Strength	psi	22,400 (154.4 MPA)
Tensile Modulus	psi	2.2 x 10 (15.17 GPa)
Tensile Elongation	%	1.49
Flexural Strength	psi	40,000
Flexural Modulus	psi	2.15 x 10 (14.82 GPa)

TABLE 2

Mechanical Properties of Continous E-Glass in

Properties	Units	Undirectional Glass/Composite
Material Density	(gm/cc)	2.06
Fiber Content by Vol.	(%)	63.4
Tensile Strength	(psi)	180,000 (1241 MPa)
Tensile Modulus	(psi)	6.93 x 10 (47.78 GPa)
Tensile Elongation	(%)	2.60
Flexural Strength	(psi)	239,000 (1647.8 MPa)
Flexural Modulus	(psi)	7.23 x 10 (49.85 GPa)
Short Beam Shear	(psi)	13,400 (92.39 MPa)
Notched IZOD Impact Strength	(ft.lb/in)	>60
Unnotched Impact Strength	(ft.lb/in)	>60 3203 Meter-Newton / Meter

7.0 INPUT LOADS

The following input loads were introduced in the analysis:

7.1 Vertical Loads

7.1.1 The normal vertical static load on each wheel equals 3500 pounds (1587.6 Kg, or 15569 Newton)

7.1.2 The maximum vertical load rating (for the steel wheel) equals 5190 lbs. (2354.2 Kg, or 23086 Newton)

7.2 Side Loads

7.2.1 The side load normal, applied at ground level, equals 1700 lbs. (771.1 Kg or 7562 Newton)

7.2.2 The maximum side load, applied at ground level, equals 2595 lbs. (1177.1 Kg or 11543 Newton)

7.2.3 The area of the load resistance is equivalent to the area of the tire in contact with the ground.

7.2.4 The maximum applied dynamic load $p = M/A \times g$
where P = applied dynamic load (pounds)

M = Maximum applied moment (ft.-lbs)

= 13,205 ft.-lbs. (17903.6 Meter-Newton)

A = Moment Arm

g = gravity loading factor based on various road terrains

7.3 Resulting Dynamic Load

The resulting maximum dynamic load is equivalent to 7,558 pounds (33620 Newton).

These loads are based on the following:

7.3.1 Wheel load rating = 5190 pounds (2354.2 Kg or 23086 Newton)

7.3.2 Coefficent of friction between tire and road M=0.70

7.3.3 Wheel offset = 3.75 inches (95.25 mm)

7.3.4 Static load radius of the tire = 20.3 inches (515.62 mm)

7.3.5 Truck width = 74.00 inches (1879.6 mm)

7.3.6 In this analysis, the composite material used in the wheel was assumed to be relatively homogeneous. The mechanical properties of this material are represented in Tables 1 and 2.

7.4 Second Loading Conditions

7.4.1 In addition, the computer program generated engineering data for a more severe loading condition. These loading conditions are:

a. The truck is at its maximum gross weight of 42,500 lbs. (19277.9 Kg)

b. The maximum vertical load on the front tire is 6000 lbs. (2721.6 Kg or 26689.3 Newton)

c. Side load applied at the ground level of tire is 2600 lbs. (1179.4 Kg or 11565.4 Newton)

d. Tire inflation pressure is 85 psi. (586 KPa)

Results of the computer analysis (in the form of stress contours) for the second loading condition are presented in Figures 18 to 31.

7.5 Third Loading Condition

7.5.1 Computer analysis for the Dynamic Cornering Fatigue was run using the following input:

7.5.1.1 The applied moment on the wheel is equivalent to 7790 ft-lbs. (10562 Meter-Newton). This load represents the design load of the wheel. A lateral load equal to 4,554 lbs. (20257 Newton) was introduced in conjunction with a moment arm equal to 3.25 ft. (0.99 Meter) This combination produces the required moment of 7790 ft-lbs.

7.5.1.2 A safety factor of 1.9 of designed load was introduced to the resultant moment as specified by the SAE, thus the torque became equivalent to 14,800 ft-lbs.

7.5.1.3 Under this inflated torque, the wheel bogie was scheduled to withstand 40,000 cycles.

7.5.1.4 The composite material used is the same as in the previous example.

The stresses in the composite wheel are plotted as stress contours throughout the surfaces of the wheel. These plots are shown in Figures 16 - 43.

7.5.2 These computer results indicate that a composite wheel based on this design can perform as required.

8.0 MANUFACTURING

Fabrication of composite wheels with the required degree of roundness and dimensional accuracy requires a well controlled production method. During the development program, several manufacturing methods were investigated. Finally, the compression molding technique was chosen because of its reliability and adaptability to future production methods.

8.1 Tooling

After the wheel and lock rim design was completed, tooling design was initiated. Based on the fact that the final mechanical properties required were quite high and that the wheel contours had to contain the tire, it was decided that each part would be manufactured by compression molding. Thus, closed die tooling was selected to achieve both the mechanical properties and the wheel shape.

8.1.1 Manufacturing Tools

A specially heated steel mold was designed, based on the finalized geometrical configuration of the composite wheel. The design and construction of the wheel mold is important, because it influences the quality, consistency, and weight of the finished product.

8.1.2 The mold was fabricated from tool steel. Well designed shear edges are necessary to insure proper sealing and minimum flash. Close tolerances were maintained at the shear edges to prevent material loss and to minimize flow orientation problems during molding. Proper heat treatment is necessary to reduce mold surface abrasion caused by contact with the wheel material, and thus to extend mold life.

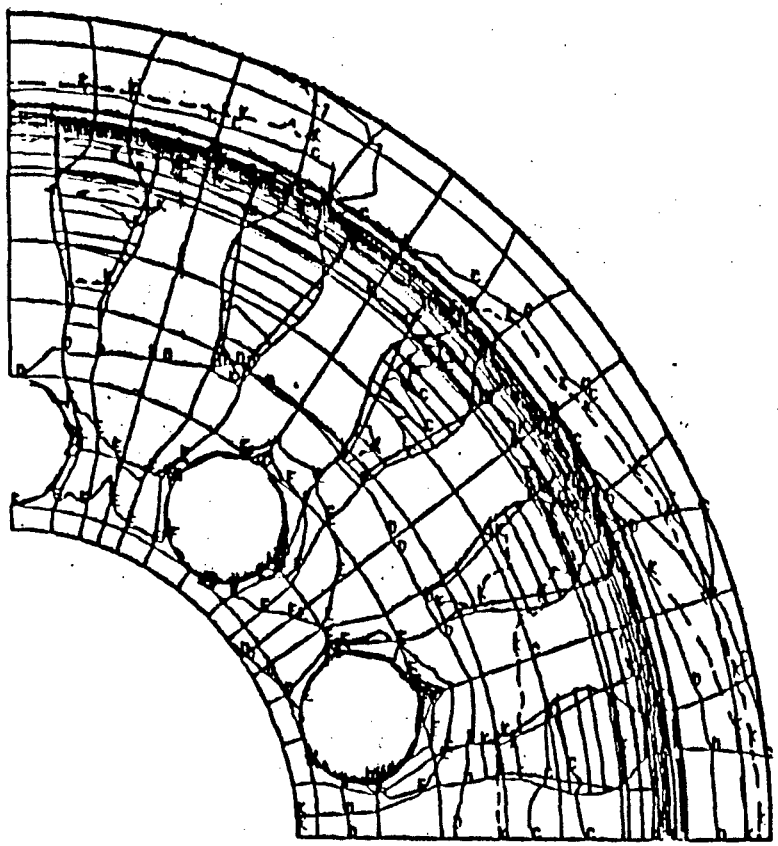

STRESS CONTOURS (P.S.I.) LOAD CASE #2		MPa
A.	8,644	59.598
B.	5,196	35.825
C.	7,494	51.669
D.	3,698	25.497
E.	8,145	56.158
F.	12,590	86.805
G.	17,840	123.002
H.	21,480	148.099
I.	25,830	178.092
J.	38,380	264.621
K.	-0-	

Figure 16 Normal Stress Contours (S_{xx}) in the Outer Surface of the Composite Wheel Due to Vertical Load Equal to 6,000 Lb. and the horizontal Load at Ground Level Equal to 2,600 Lb. with a Tire Pressure of 85 P.S.I. (586 KPa)

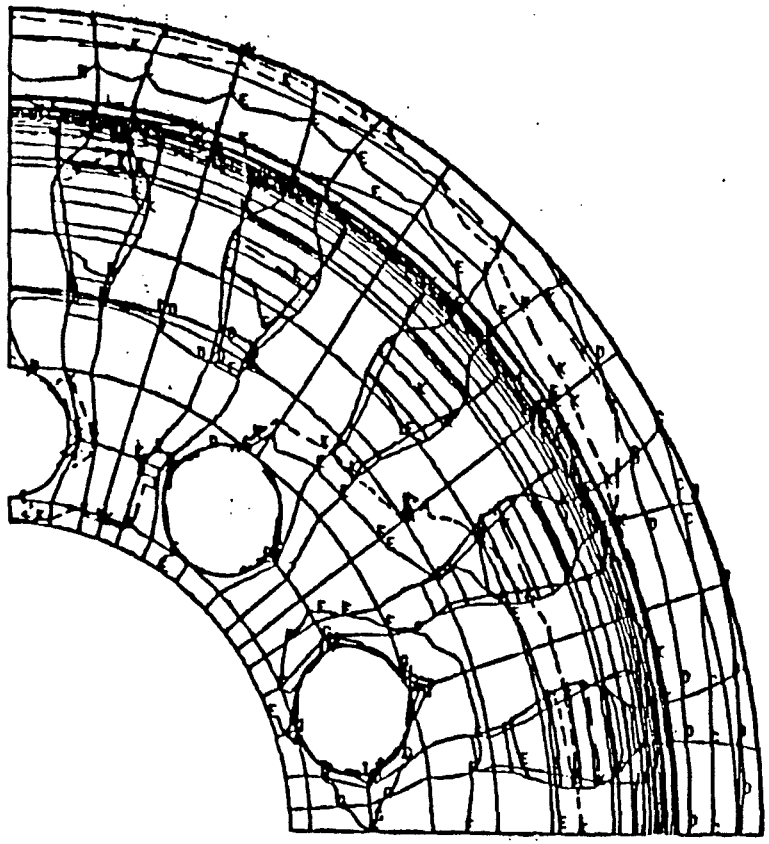

STRESS CONTOURS (P.S.I.) LOAD CASE #2		MPa
A.	19,430	133.965
B.	14,180	97.768
C.	8,953	61.729
D.	3,713	25.600
E.	1,527	10.528
F.	8,787	60.584
G.	12,880	88.804
H.	17,240	118.866
I.	22,480	154.994
J.	27,720	191.123
K.	-0-	

Figure 17 Normal Stress Contours (S_{yy}) in the Outer Surface of the Composite Wheel Due to Vertical Load Equal to 6,000 Lb. and the horizontal Load at Ground Level Equal to 2,600 Lb. with a Tire Pressure of 85 P.S.I.

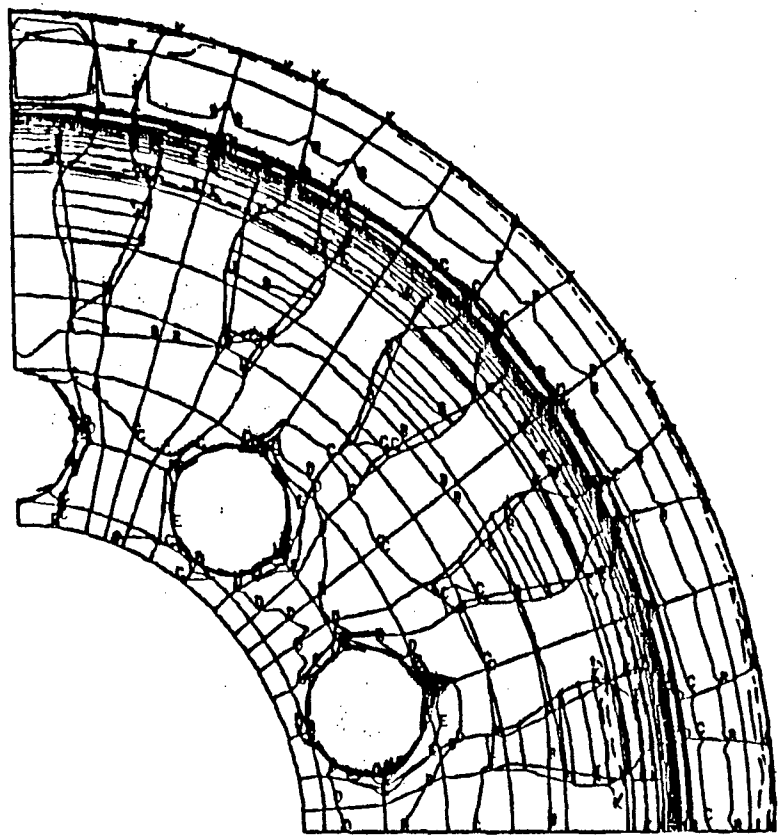

STRESS CONTOURS (P.S.I.) LOAD CASE #2		MPa
A.	6,788	46.802
B.	3,247	22.387
C.	7,174	49.463
D.	11,180	77.083
E.	15,820	109.075
F.	18,950	130.656
G.	22,880	157.752
H.	28,810	198.638
I.	38,730	267.034
J.	34,880	240.489
K.	-0-	

Figure 18 Maximum Principal Stress Contours (S_3) in the Outer Surface of the Composite Wheel due to Vertical Load Equal to 6,000 lbs. and the Horizontal Load at Ground Level Equal to 2,600 lbs. with a Tire Pressure of 85 P.S.I.

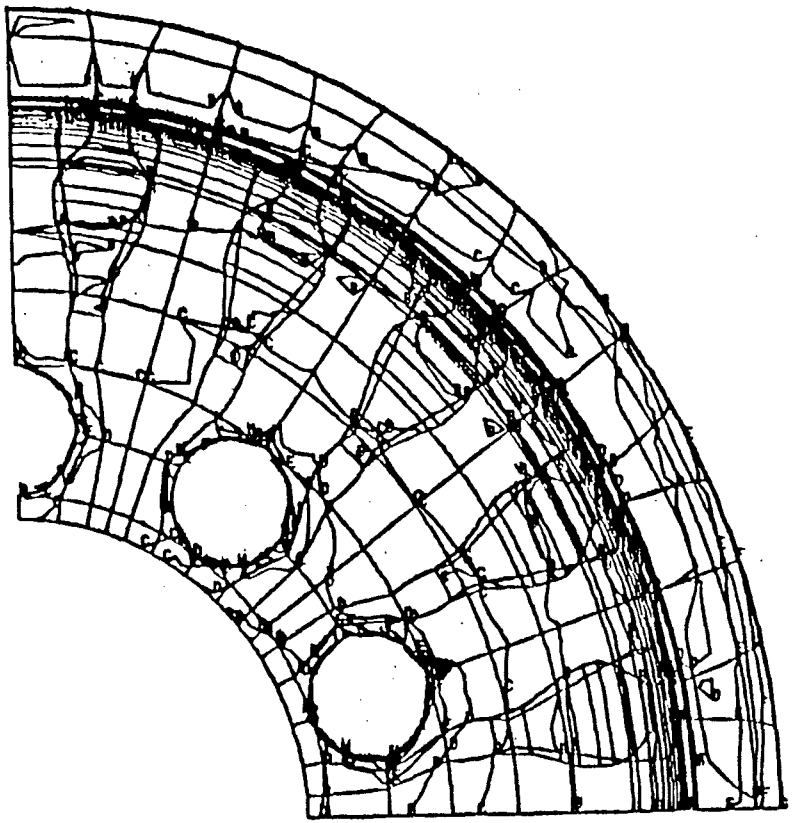

STRESS CONTOURS (P.S.I.) LOAD CASE #2		MPa
A.	4,292	29.592
B.	3,449	23.780
C.	6,478	44.664
D.	8,498	58.592
E.	12,510	86.253
F.	15,530	107.076
G.	18,550	127.898
H.	21,570	148.720
I.	24,590	169.542
J.	27,610	190.364
K.	-0-	

Figure 19 Von Mises Equivalent Stress Contours (S_{Eg}) in the Outer Surface of the Composite Wheel due to Horizontal Load Equal to 6,000 lbs. and the Horizontal Load at Ground Level Equal to 2,600 lbs. with a Tire Pressure of 85 P.S.I.

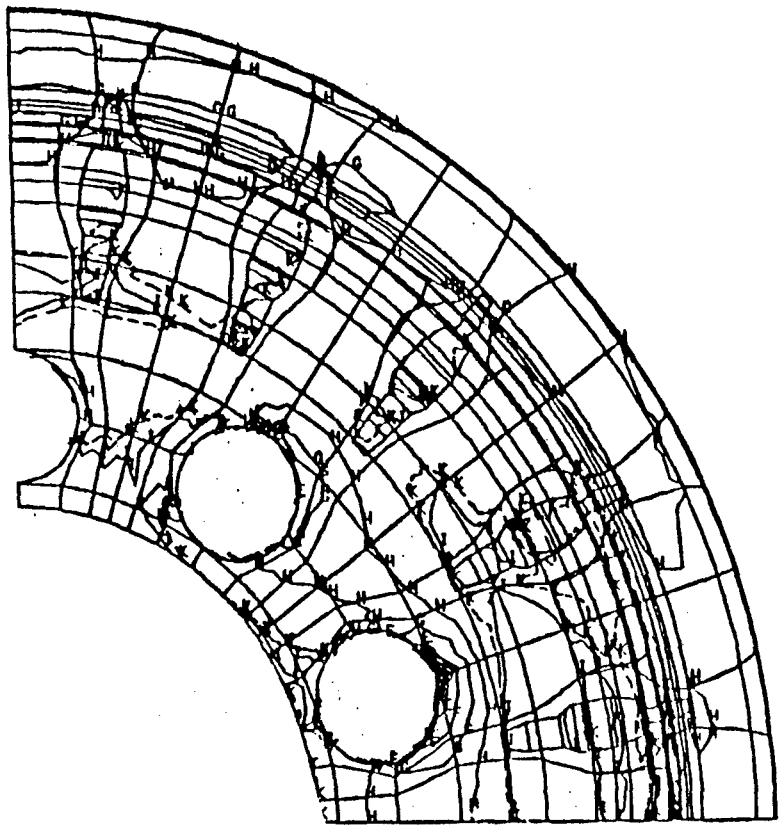

STRESS CONTOURS (P.S.I.) LOAD CASE #2		MPa
A.	34,540	238.145
B.	38,170	263.173
C.	25,880	178.436
D.	21,490	148.168
E.	17,860	123.140
F.	12,690	87.494
G.	83,310	574.402
H.	3,962	27.317
I.	4,857	33.488
J.	4,774	32.916
K.	-0-	

Figure 20 Normal Stress Contours (S_{xx}) in the Inner Surface of the Composite Wheel due to Vertical Load Equal to 6,000 lbs. and the Horizontal Load at Ground Level Equal to 2,600 lbs. with a Tire Pressure of 85 P.S.I.

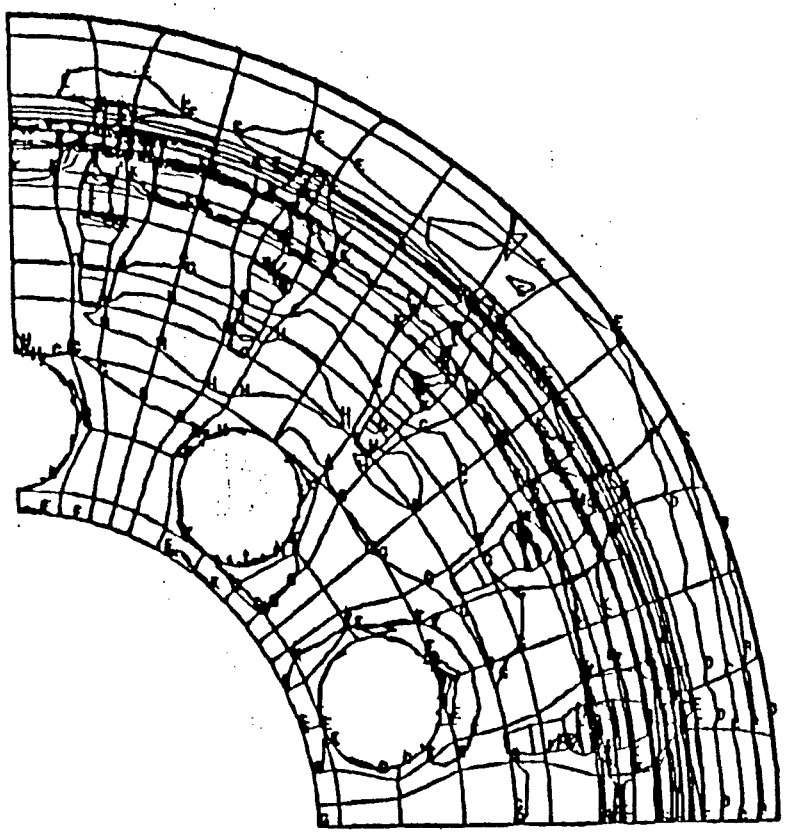

STRESS CONTOURS (P.S.I.) LOAD CASE #2		MPa
A.	14,860	102.456
B.	11,230	77.428
C.	8,418	58.040
D.	5,585	38.507
E.	2,768	19.085
F.	8,511	58.681
G.	2,898	19.981
H.	5,715	39.404
I.	8,541	58.888
J.	11,380	78.462
K.	-0-	

Figure 21 Normal Stress Contours (S_{yy}) in the Inner Surface of the Composite Wheel due to Vertical Load Equal to 6,000 lbs. and the Horizontal Load at Ground Level Equal to 2,600 lbs. with a Tire Pressure of 85 P.S.I.

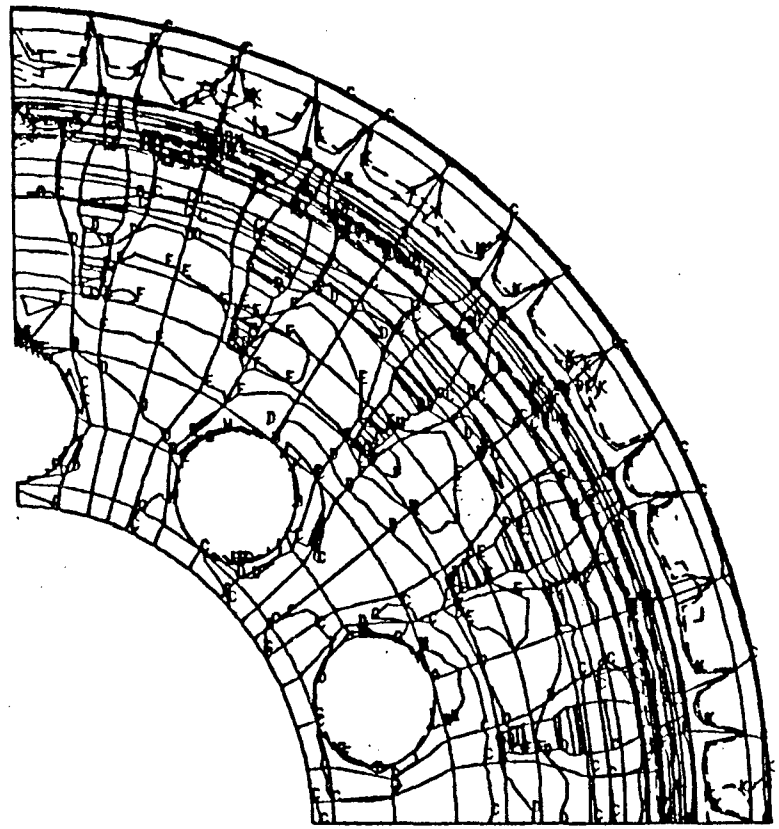

STRESS CONTOURS (P.S.I.) LOAD CASE #2		MPa
A.	2,375	16.375
B.	7,938	54.731
C.	2,217	15.286
D.	4,513	31.116
E.	6,818	47.008
F.	9,188	63.349
G.	11,480	79.152
H.	13,690	94.389
I.	15,990	110.247
J.	18,290	126.105
K.	-0-	

Figure 22 Maximum Principal Stress Contours (S_3) in the Inner Surface of the Composite Wheel due to Vertical Load Equal to 6,000 lbs. and the Horizontal Load at Ground Level Equal to 2,600 lbs. with a Tire Pressure of 85 P.S.I.

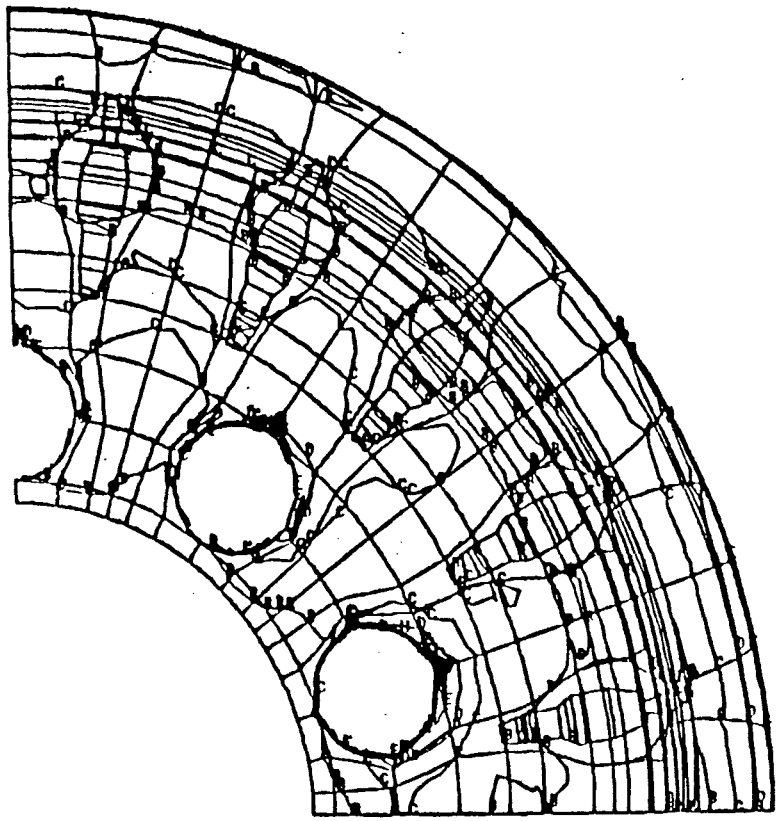

STRESS CONTOURS (P.S.I.) LOAD CASE #2		MPa
A.	3,928	27.083
B.	4,847	33.419
C.	7,783	53.662
D.	11,950	82.392
E.	15,810	109.006
F.	18,870	130.104
G.	22,320	153.891
H.	25,980	179.126
I.	28,830	198.776
J.	33,290	229.526
K.	-0-	

Figure 23 Von Mises Equivalent Stress Contours (S_{Eq}) in the Inner Surface of the Composite Wheel due to Vertical Load Equal to 6,000 lbs. and the Horizontal Load at Ground Level Equal to 2,600 lbs. with a Tire Pressure of 85 P.S.I.

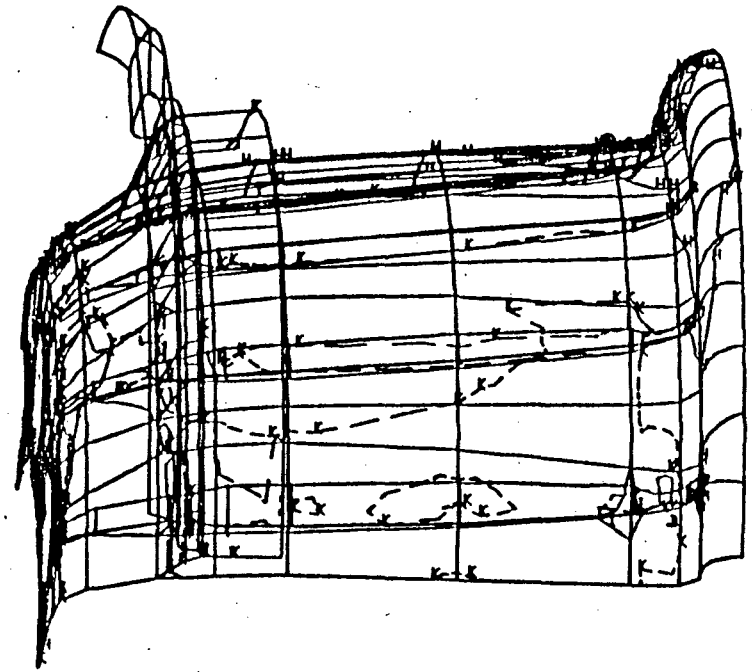

STRESS CONTOURS (P.S.I.) LOAD CASE #2		MPa
A.	34,540	238.145
B.	30,170	208.015
C.	25,800	177.885
D.	21,430	147.755
E.	17,860	123.140
F.	12,690	87.494
G.	8,331	57.440
H.	3,962	27.317
I.	4,057	27.972
J.	4,774	32.916
K.	-0-	

Figure 24 Normal Stress Contours (S_{xx}) in the Bottom Surface of the Composite Wheel Rim due to Vertical Load Equal to 6,000 lbs. and the Horizontal Load at Ground Level Equal to 2,600 lbs. with a Tire Pressure of 85 P.S.I.

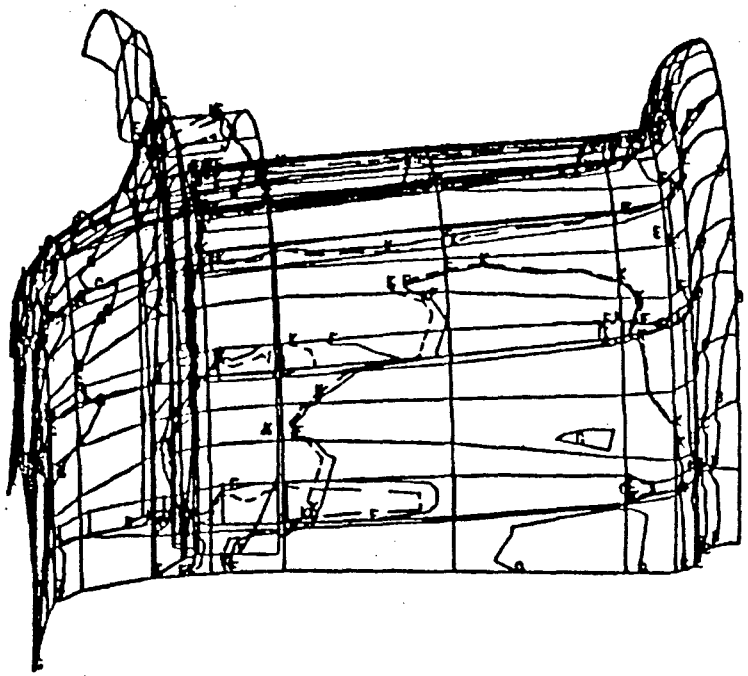

STRESS CONTOURS (P.S.I.) LOAD CASE #2		MPa
A.	14,860	102.456
B.	11,230	77.428
C.	8,410	57.985
D.	5,585	38.507
E.	2,760	19.030
F.	6,511	44.892
G.	2,890	19.926
H.	5,715	39.404
I.	8,541	58.888
J.	11,360	78.324
K.	-0-	

Figure 25 Normal Stress Contours (S_{yy}) in the Bottom Surface of the Composite Wheel Rim due to Vertical Load Equal to 6,000 lbs. and the Horizontal Load at Ground Level Equal to 2,600 lbs. with a Tire Pressure of 85 P.S.I.

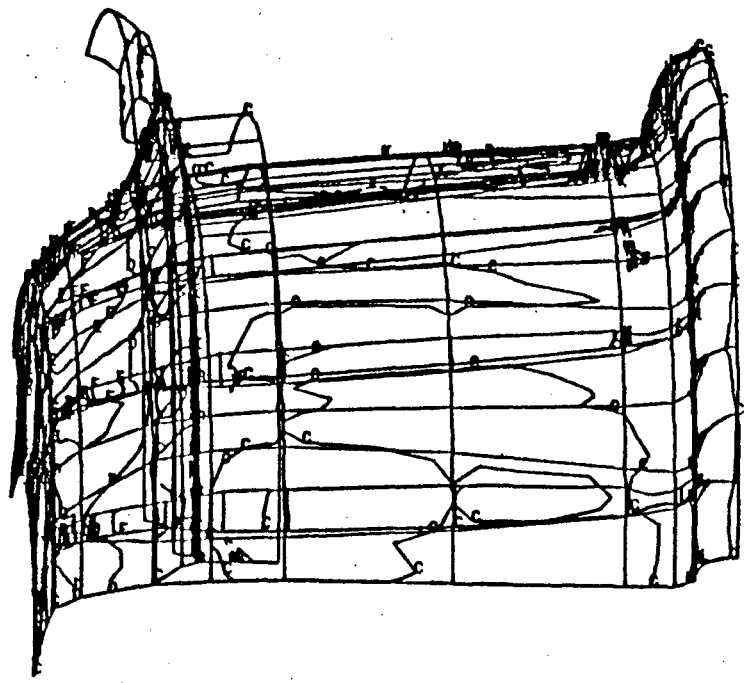

STRESS CONTOURS (P.S.I.) LOAD CASE #2		MPa
A.	2,375	16.375
B.	7,936	54.717
C.	2,217	15.286
D.	4,513	31.116
E.	6,810	46.953
F.	9,106	62.784
G.	11,400	78.600
H.	13,690	94.389
I.	15,990	110.247
J.	18,290	126.105
K.	-0-	

Figure 26 Maximum Principal Stress Contours (S_3) in the Bottom Surface of the Composite Wheel Rim due to Vertical Load Equal to 6,000 lbs. and the Horizontal Load at Ground Level Equal to 2,600 lbs. with a Tire Pressure of 85 P.S.I.

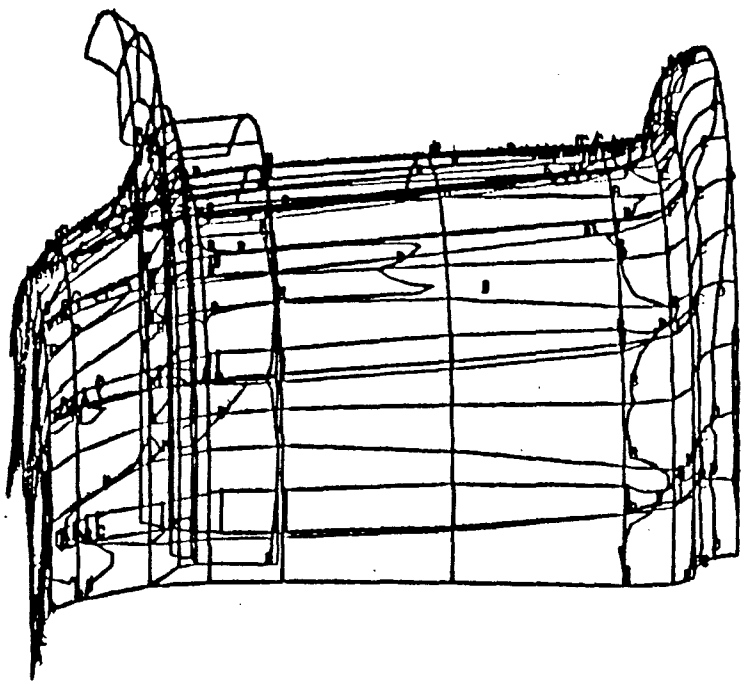

STRESS CONTOURS (P.S.I.) LOAD CASE #2		MPa
A.	3,920	27.027
B.	4,047	27.903
C.	7,703	53.110
D.	11,350	78.255
E.	15,810	109.006
F.	18,670	128.725
G.	22,320	153.891
H.	25,980	179.126
I.	29,630	204.292
J.	33,290	229.526
K.	-0-	

Figure 27 Von Mises Equivalent Stress Contours (S_{Eq}) in the Bottom Surface of the Composite Wheel Rim due to Vertical Load Equal to 6,000 lbs. and the Horizontal Load at Ground Level Equal to 2,600 lbs. with a Tire Pressure of 85 P.S.I.

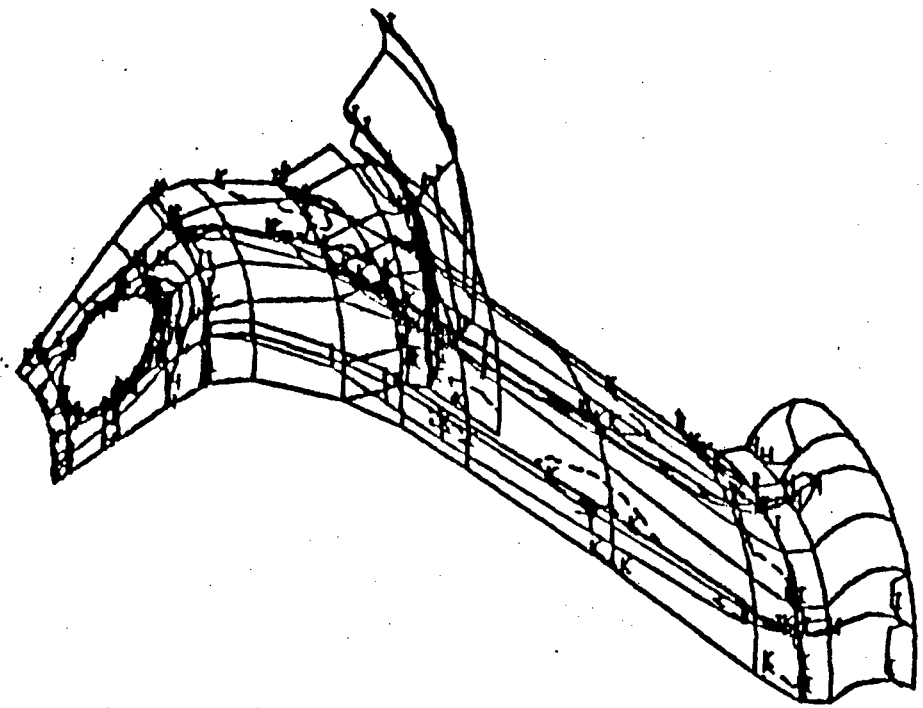

STRESS CONTOURS (P.S.I.) LOAD CASE #2		MPa
A.	34,540	238.145
B.	30,320	209.049
C.	28,110	193.812
D.	21,980	151.547
E.	17,680	121.899
F.	13,470	92.872
G.	9,258	63.832
H.	5,844	40.293
I.	8,380	57.778
J.	3,384	23.332
K.	-0-	

Figure 28 Normal Stress Contours (S_{xx}) Around the Bolt Holes in the Composite Wheel Rim due to Vertical Load Equal to 6,000 lbs. and the Horizontal Load at Ground Level Equal to 2,600 lbs. with a Tire Pressure of 85 P.S.I.

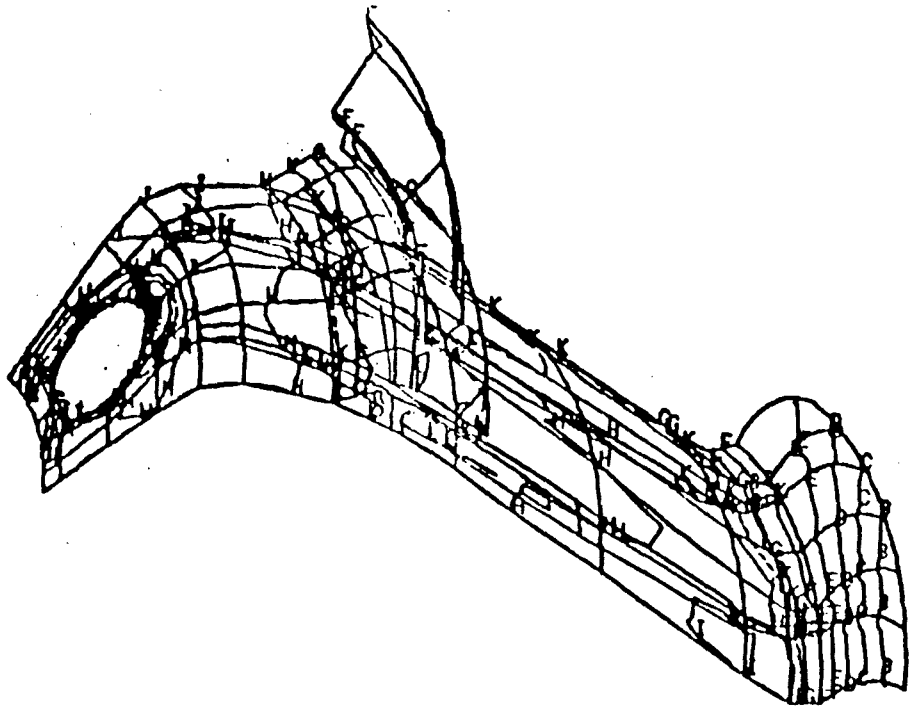

STRESS CONTOURS (P.S.I.) LOAD CASE #2		MPa
A.	14,860	102.456
B.	11,860	81.772
C.	9,876	68.093
D.	7,483	51.593
E.	5,291	36.480
F.	3,898	26.876
G.	9,857	67.962
H.	1,286	8.867
I.	3,479	23.987
J.	5,672	39.107
K.	-0-	

Figure 29 Normal Stress Contours (S_{yy}) Around the Bolt Holes in the Composite Wheel Rim due to Vertical Load Equal to 6,000 lbs. and the Horizontal Load at Ground Level Equal to 2,600 lbs. with a Tire Pressure of 85 P.S.I.

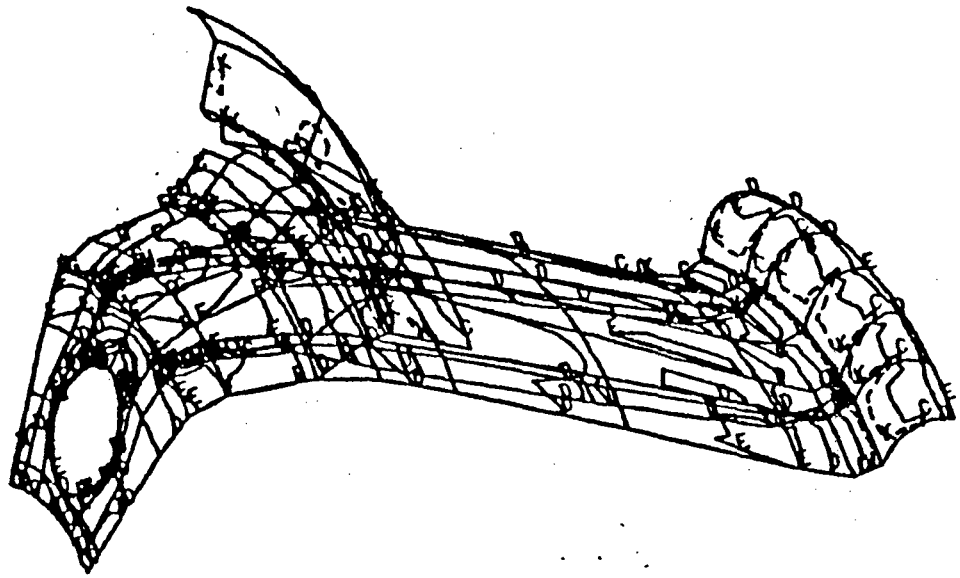

STRESS CONTOURS (P.S.I.) LOAD CASE #2		MPa
A.	2,375	16.375
B.	9,883	68.141
C.	5,752	39.659
D.	2,858	19.705
E.	3,526	24.311
F.	5,882	40.555
G.	6,477	44.657
H.	7,953	54.834
I.	9,428	65.004
J.	18,900	130.311
K.	-0-	

Figure 30 Maximum Principal Stress Contours (S_3) Around the Bolt Holes in the Composite Wheel Rim due to Vertical Load Equal to 6,000 lbs. and the Horizontal Load at Ground Level Equal to 2,600 lbs. with a Tire Pressure of 85 P.S.I.

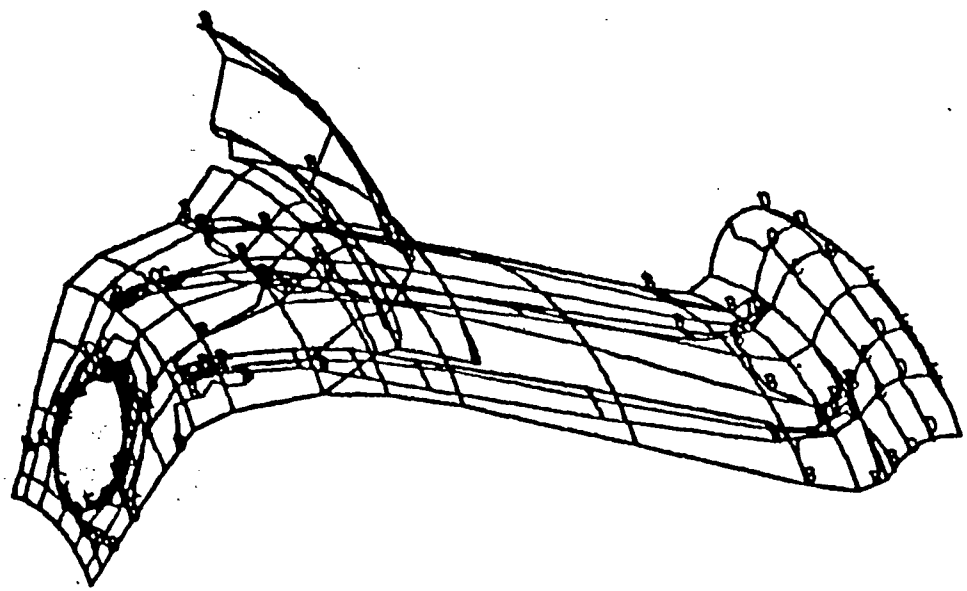

STRESS CONTOURS (P.S.I.) LOAD CASE #2		MPa
A.	6,138	42.320
B.	4,244	29.261
C.	7,875	54.296
D.	11,580	79.841
E.	15,130	104.318
F.	18,760	129.346
G.	22,480	154.994
H.	26,830	184.986
I.	29,680	204.636
J.	33,280	229.457
K.	-0-	

Figure 31 Von Mises Equivalent Stress Contours (S_{Eq}) Around the Bolt Holes in the Composite Wheel due to Vertical Load Equal to 6,000 lbs. and the Horizontal Load at Ground Level Equal to 2,600 lbs. with a Tire Pressure of 85 P.S.I.

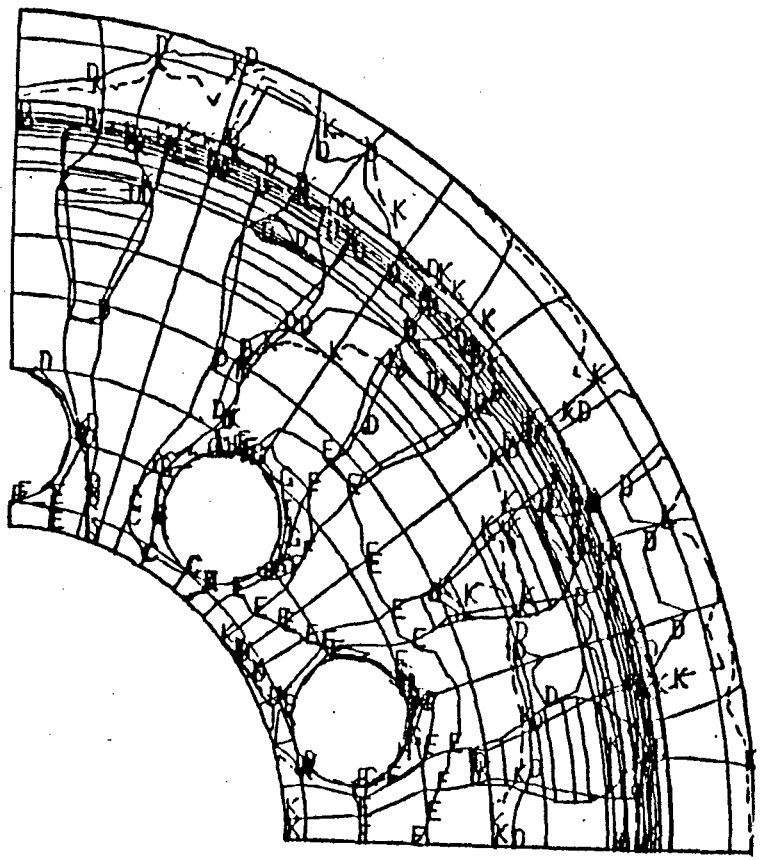

Figure 32 Normal Stress Contours (S_{xx}) in the Outer Surface of the Composite Wheel due to Cornering Fatique Loads.

STRESS CONTOURS IDENTIFICATION

	Torque = 7,790 Ft. Lb. Psi	MPa	Torque = 14,800 Ft. Lb. Psi	Mpa
A.	13,445	92.700	25,538	176.078
B.	8,069	55.634	15,327	105.676
C.	4,619	31.847	8,773	60.488
D.	234	1.613	444	3.061
E.	4,142	28.558	7,868	54.248
F.	8,527	58.792	16,197	111.674
G.	12,978	89.480	24,651	169.963
H.	17,279	119.134	32,820	226.286
I.	21,664	149.368	41,150	283.719
J.	26,040	179.539	4,946	34.105
K.	-0-		-0-	

Torque = 7,790 Ft. Lbs. (10562 Meter-Newton)
and = 14,800 Ft. Lbs. (20066 Meter-Newton)

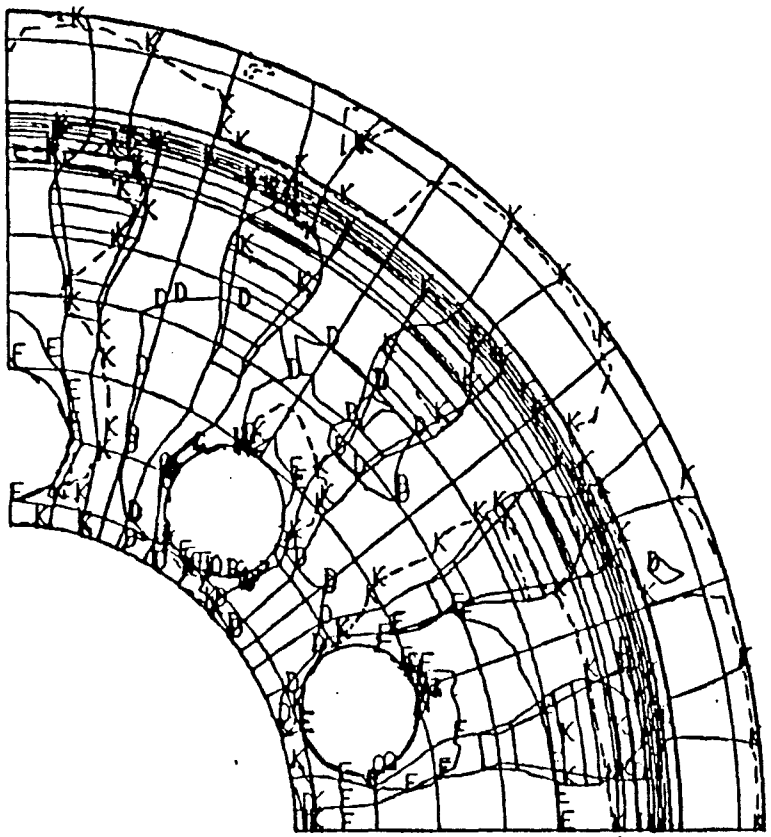

STRESS CONTOURS IDENTIFICATION

	Torque = 7,790 Ft. Lb. Psi	MPa	Torque = 14,800 Ft. Lb. Psi	Mpa
A.	8,265	56.985	15,699	108.241
B.	5,750	39.645	1,092	7.529
C.	3,244	22.367	6,163	42.492
D.	729	5.026	1,385	9.549
E.	1,777	12.252	337	2.324
F.	4,282	29.523	8,134	56.082
G.	6,816	46.995	12,947	89.266
H.	9,303	64.142	1,767	12.183
I.	11,996	82.710	22,786	157.104
J.	14,324	98.760	27,208	187.593
K.	-0-		-0-	

Torque = 7,790 Ft. Lbs.
and = 14,800 Ft. Lbs.

Figure 33 Normal Stress Contours (S_{yy}) in the Outer Surface of the Composite Wheel due to Cornering Fatique Loads.

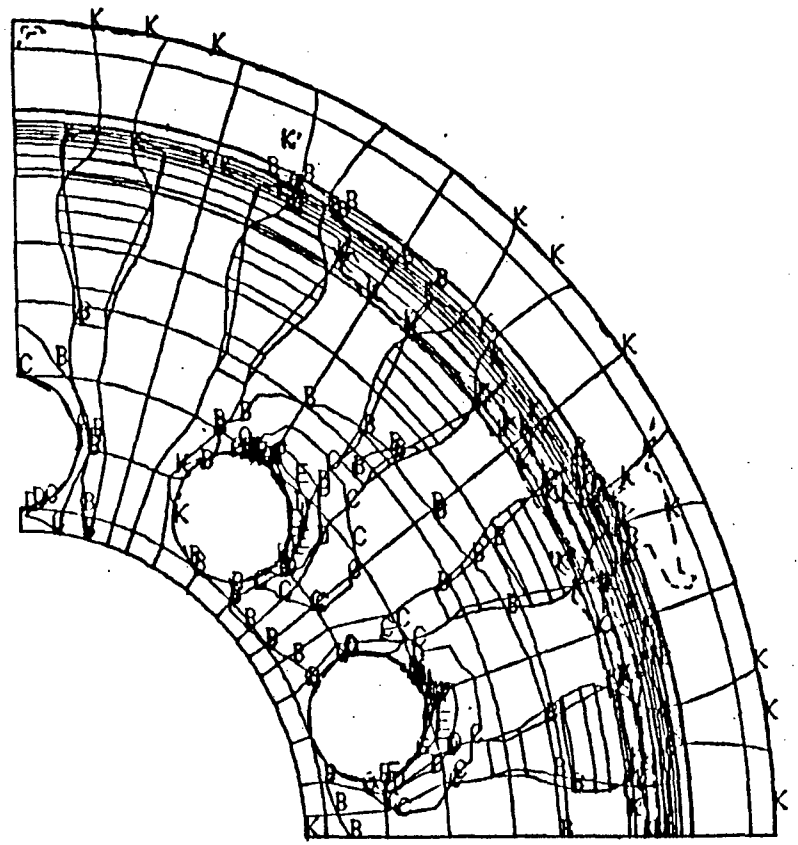

STRESS CONTOURS IDENTIFICATION

	Torque = 7,790 Ft. Lbs. Psi	MPa	Torque = 14,800 Ft. Lbs. Psi	Mpa
A.	1,300	8.963	2,469	17.023
B.	2,235	15.410	4,245	29.268
C.	5,535	38.162	10,514	72.491
D.	8,901	61.370	16,908	116.577
E.	12,267	84.578	23,301	160.655
F.	17,513	120.748	33,264	229.347
G.	27,059	186.565	51,397	354.370
H.	22,384	154.332	42,517	293.144
I.	25,759	177.602	4,893	33.736
J.	29,135	200.879	55,340	381.556
K.	-0-		-0-	

Torque = 7,790 Ft. Lbs.
and = 14,800 Ft. Lbs.

Figure 34 Maximum Principal Stress Contours (S_3) in the Outer Surface of the Composite Wheel due to Cornering Fatique Loads.

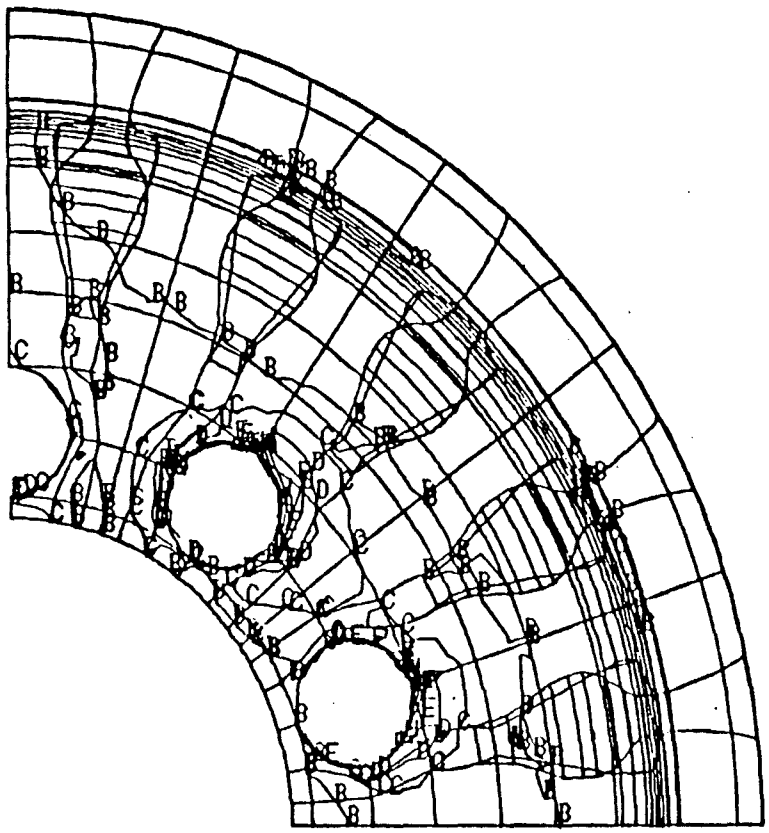

STRESS CONTOURS IDENTIFICATION

	Torque = 7,790 Ft. Lbs. Psi	MPa	Torque = 14,800 Ft. Lbs. Psi	Mpa
A.	-0-		-0-	
B.	2,702	18.630	5,133	35.391
C.	5,507	37.969	10,460	72.119
D.	8,817	60.791	14,972	103.228
E.	10,509	72.457	19,962	137.633
F.	13,885	95.734	26,374	181.842
G.	15,764	108.689	29,943	206.450
H.	18,391	126.801	34,934	240.861
I.	21,019	144.921	39,924	275.266
J.	23,646	163.033	44,915	309.678
K.	-0-		-0-	

Torque = 7,790 Ft. Lbs.
and = 14,800 Ft. Lbs.

Figure 35 Von Mises Equivalent Stress Contours (S_{Eg}) in the Outer Surface of the Composite Wheel due to Cornering Fatique Loads.

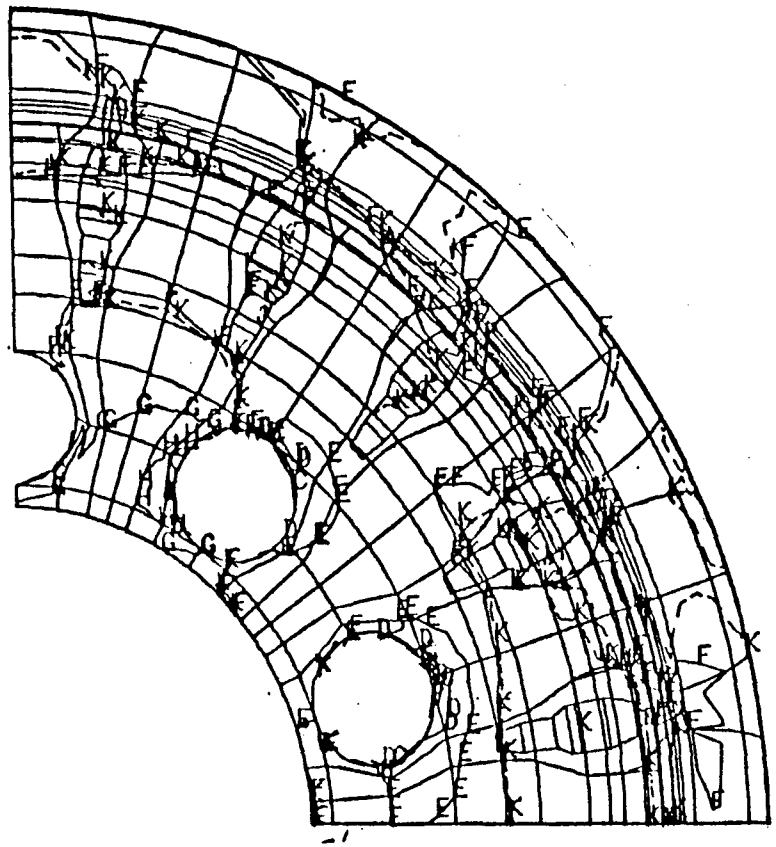

STRESS CONTOURS IDENTIFICATION

	Torque = 7,790 Ft. Lb. Psi	MPa	Torque = 14,800 Ft. Lb. Psi	Mpa
A.	25,114	173.155	47,703	328.901
B.	27,012	186.241	51,309	353.763
C.	14,698	101.339	27,919	192.495
D.	17,344	119.583	32,945	227.148
E.	5,030	34.681	9,555	65.879
F.	271	1.868	515	3.551
G.	4,638	31.978	8,809	60.736
H.	16,952	116.880	32,199	222.004
I.	14,380	99.147	27,315	188.330
J.	26,619	183.532	50,563	348.620
K.	-0-		-0-	

Torque = 7,790 Ft. Lbs.
and = 14,800 Ft. Lbs.

Figure 36 Normal Stress Contours (S_{xx}) in the Inner Surface of the Composite Wheel due to Cornering Fatique Loads.

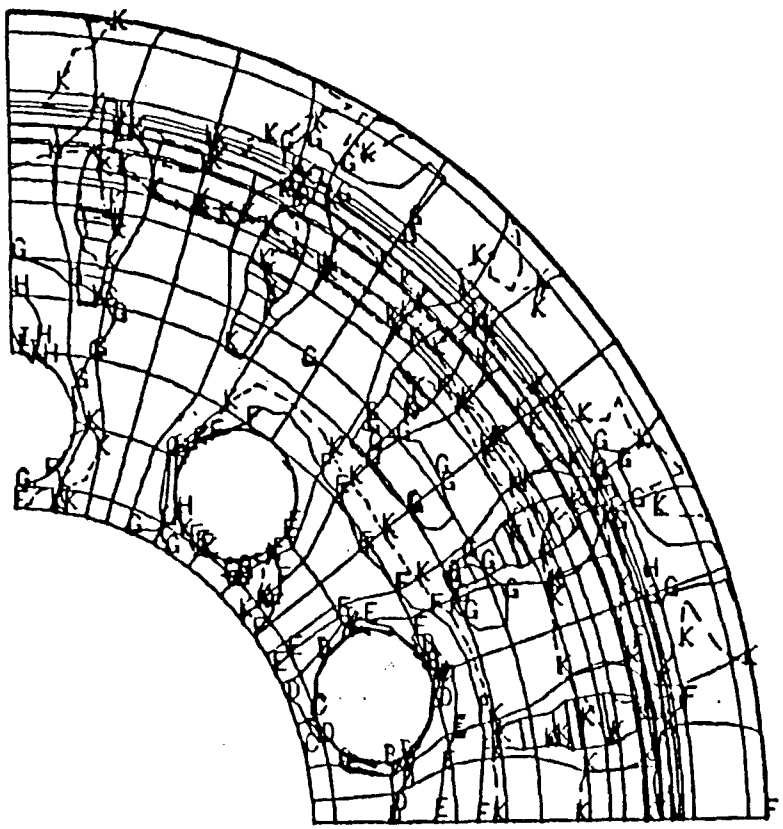

STRESS CONTOURS IDENTIFICATION

	Torque = 7,790 Ft. Lbs. Psi	MPa	Torque = 14,800 Ft. Lbs. Psi	Mpa
A.	17,475	120.468	33,193	228.858
B.	8,143	56.144	15,469	106.655
C.	6,293	43.389	11,970	82.530
D.	4,432	30.558	8,472	58.412
E.	2,599	17.919	4,937	34.039
F.	832	5.736	1,581	10.901
G.	1,094	7.543	2,078	14.327
H.	8,555	58.985	16,250	112.040
I.	4,797	33.074	9,111	62.818
J.	6,723	46.353	12,752	87.922
K.	-0-		-0-	

Torque = 7,790 Ft. Lbs.
and = 14,800 Ft. Lbs.

Figure 37 Normal Stress Contours (S_{yy}) in the Inner Surface of the Composite Wheel due to Cornering Fatique Loads.

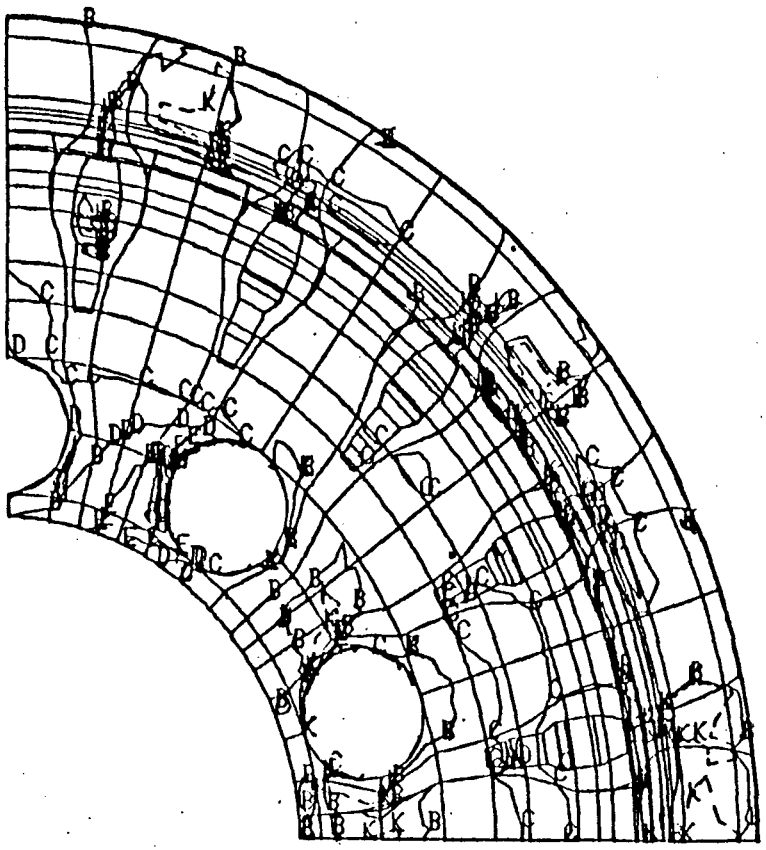

STRESS CONTOURS IDENTIFICATION

	Torque = 7,790 Ft. Lbs. Psi	MPa	Torque = 14,800 Ft. Lbs. Psi	Mpa
A.	2,730	18.823	5,186	35.756
B.	85,777	591.412	162,930	1123.363
C.	2,776	19.140	5,275	36.370
D.	5,535	38.162	10,514	72.491
E.	8,284	57.116	15,735	108.489
F.	11,108	76.587	21,099	145.472
G.	13,782	95.024	26,178	180.491
H.	16,531	113.977	31,400	216.495
I.	26,769	184.566	50,847	350.578
J.	27,648	190.626	52,516	362.085
K.	-0-		-0-	

Torque = 7,790 Ft. Lbs.
and = 14,800 Ft. Lbs.

Figure 38 Maximum Principal Stress Contours (S_3) in the Inner Surface of the Composite Wheel due to Cornering Fatique Loads.

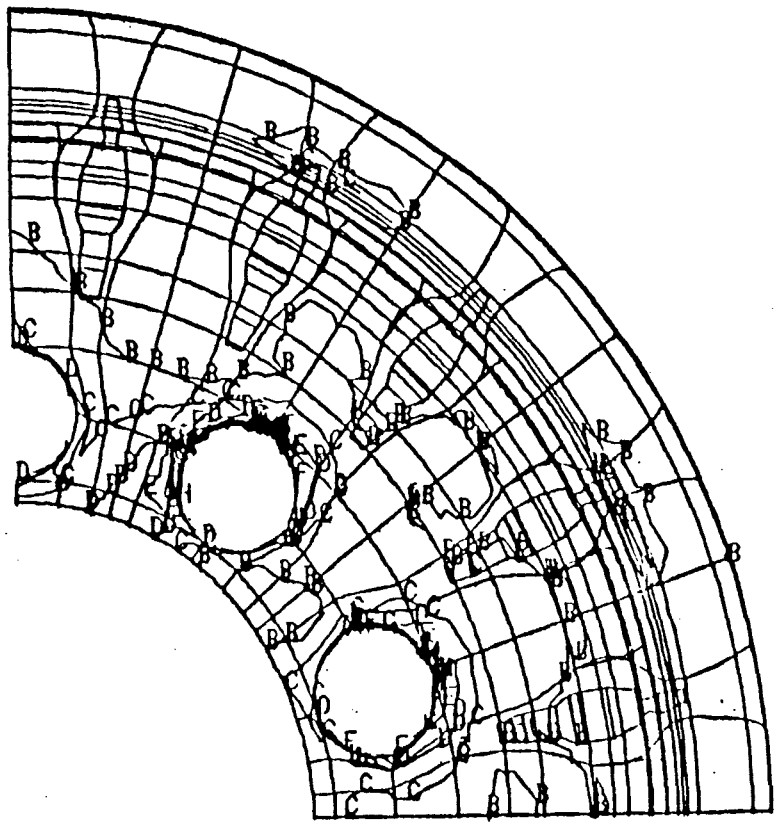

STRESS CONTOURS IDENTIFICATION

	Torque = 7,790 Ft. Lbs. Psi	MPa	Torque = 14,800 Ft. Lbs. Psi	Mpa
A.	-O-		-O-	
B.	2,543	17.533	4,831	33.309
C.	5,086	35.067	9,661	66.610
D.	7,648	52.731	14,528	100.167
E.	17,652	121.706	33,531	231.188
F.	18,588	128.160	35,307	243.433
G.	17,129	118.100	32,536	224.328
H.	18,550	127.898	35,236	242.944
I.	20,355	140.343	38,664	266.579
J.	22,898	157.876	43,494	299.881
K.	-O-		-O-	

Torque = 7,790 Ft. Lbs.
and = 14,800 Ft. Lbs.

Figure 39 Von Mises Equivalent Stress Contours (S_{Eg}) in the Inner Surface of the Composite Wheel due to Cornering Fatique Loads.

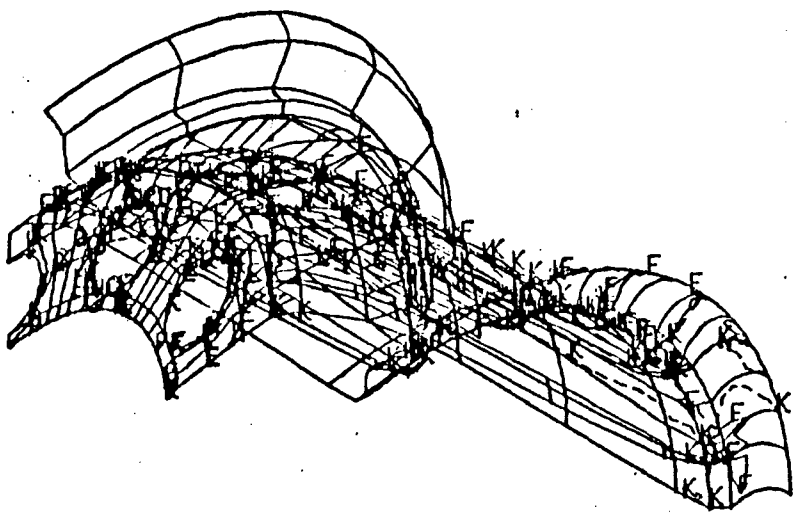

STRESS CONTOURS IDENTIFICATION

	Torque = 7,790 Ft. Lbs. Psi	MPa	Torque = 14,800 Ft. Lbs. Psi	Mpa
A.	-0-		-0-	
B.	27,012	186.241	51,309	353.763
C.	14,698	101.339	27,919	192.495
D.	17,344	119.583	32,945	227.148
E.	5,030	34.681	9,555	65.879
F.	272	1.875	515	3.551
G.	4,638	31.978	8,809	60.736
H.	16,952	116.880	35,199	222.004
I.	14,380	99.147	27,315	188.330
J.	26,619	183.532	50,563	348.620
K.	-0-		-0-	

Torque = 7,790 Ft. Lbs.
and = 14,800 Ft. Lbs.

Figure 40 Normal Stress Contours (S_{XX}) in the Bottom Surface of the Composite Wheel Rim due to Cornering Fatique Loads.

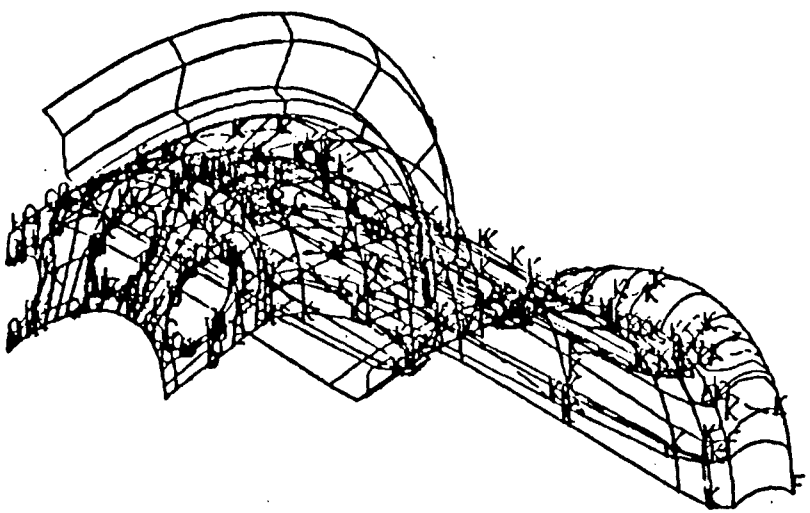

STRESS CONTOURS IDENTIFICATION

	Torque = 7,790 Ft. Lbs.		Torque = 14,800 Ft. Lbs.	
	Psi	MPa	Psi	Mpa
A.	17,662	121.775	33,549	231.312
B.	8,143	56.144	15,469	106.655
C.	630	4.344	11,970	82.530
D.	4,479	30.882	8,507	58.654
E.	260	1.793	4,937	34.039
F.	832	5.736	1,581	10.901
G.	1,094	7.543	2,078	14.327
H.	2,945	20.305	5,594	38.569
I.	4,797	33.074	9,111	62.818
J.	6,723	46.353	12,769	88.039
K.	-0-		-0-	

Torque = 7,790 Ft. Lbs.
and = 14,800 Ft. Lbs.

Figure 41 Normal Stress Contours (S_{yy}) in the Bottom Surface of the Composite Wheel Rim due to Cornering Fatique Loads.

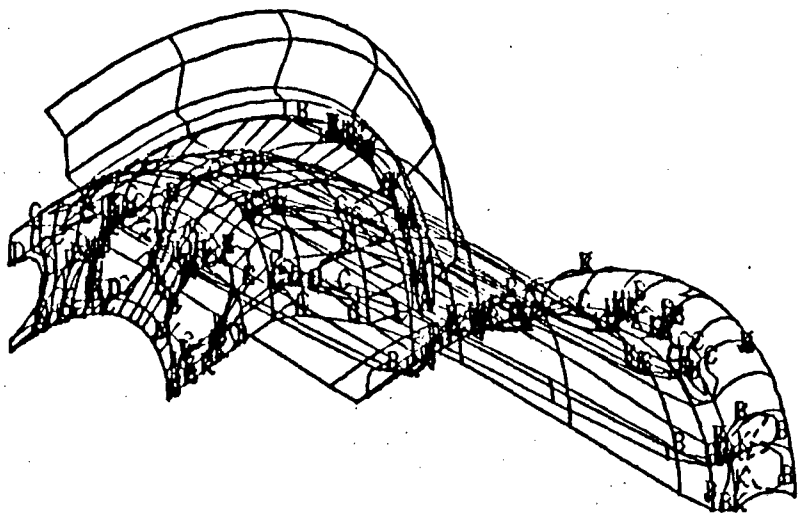

STRESS CONTOURS IDENTIFICATION

	Torque = 7,790 Ft. Lbs. Psi	MPa	Torque = 14,800 Ft. Lbs. Psi	Mpa
A.	2,731	18.83	5,186	35.756
B.	2,964	20.436	5,630	38.817
C.	2,777	19.147	5,275	36.370
D.	5,535	38.162	10,514	72.491
E.	828	5.709	15,735	108.489
F.	11,108	76.587	21,099	145.472
G.	13,782	95.024	36,175	249.418
H.	16,718	115.267	31,755	218.943
I.	26,769	184.566	50,847	350.578
J.	22,038	151.947	41,860	288.615
K.	-0-		-0-	

Torque = 7,790 Ft. Lbs.
and = 14,800 Ft. Lbs.

Figure 42 Maximum Principal Stress Contours (S_3) in the Bottom Surface of the Composite Wheel Rim due to Cornering Fatique Loads.

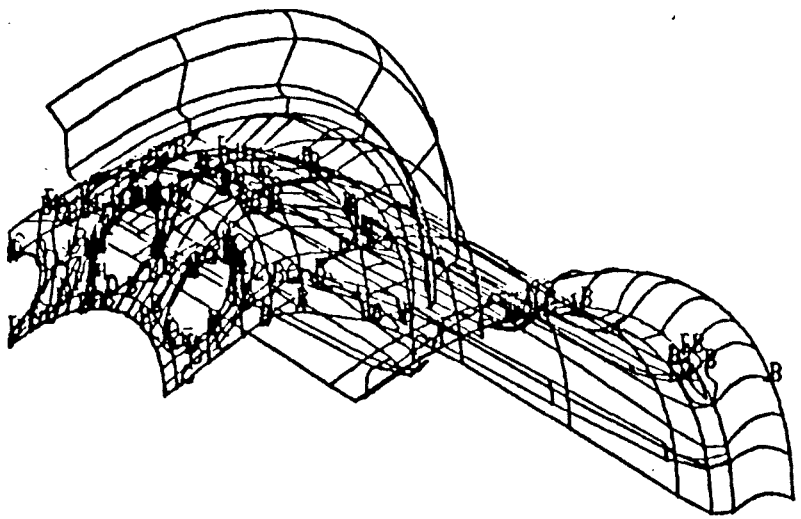

STRESS CONTOURS IDENTIFICATION

	Torque = 7,790 Ft. Lbs. Psi	MPa	Torque = 14,800 Ft. Lbs. Psi	Mpa
A.	-0-		-0-	
B.	2,543	17.533	4,830	33.302
C.	5,086	35.067	9,661	66.610
D.	7,630	52.607	14,492	99.919
E.	17,653	121.713	33,539	231.243
F.	12,791	88.191	24,295	167.508
G.	15,259	105.207	28,984	199.838
H.	18,550	127.898	35,236	242.944
I.	20,354	140.336	38,664	266.579
J.	22,898	157.876	43,494	299.881
K.	-0-		-0-	

Torque = 7,790 Ft. Lbs.
and = 14,800 Ft. Lbs.

Figure 43 Von Mises Equivalent Stress Contours (S_{eq}) in the Bottom Surface of the Composite Wheel Rim due to Cornering Fatique Loads.

8.1.3 The wheel mold consisted of three basic units:

8.1.3.1 The female cavity

8.1.3.2 The male plunger

8.1.3.3 Sliding side blocks activated by hydraulic cylinders

8.1.4 A schematic of the basic wheel mold is shown in Figure 44. The tool is equipped with ejection pins activated by an ejection plate for part removal from the mold.

8.1.5 Since the design requires that the disc and rim assembly be fabricated as an integral unit, and the side ring to be fabricated separately, another steel tool for the side ring was designed and fabricated. This tool was simpler than the disc/rim tool.

8.1.6 Tool steel was used to fabricate the side ring mold. Like the disc/rim mold, proper shear edges and core heating are required. The same quality necessary for the disc/rim mold is also required for the side ring mold. All other tool details are similar to what has been discussed above.

8.1.7 The dies were tried out using various sized charges. By trial and error, the proper charge size was determined.

The ring mold was charged with HMC compound in the main cavity. These rings were tested and then changed to high strength molding compound (XMC). These rings had long directional glass fibers in areas of high stress concentration.

8.2 Manufacturing Approach

To fabricate a truck wheel with the required roundness and dimensional accuracy, a highly controlled production process was adopted. During the program, compression molding was chosen due to its flexibility and adaptability to future production systems.

8.3 Manufacturing Technique

The manufacturing process for metal wheels usually involves stamping, forging, and welding. Each of these processes can produce nonuniformities such as eccentricity and runout. Eccentricity is defined as a measure of the amount that the hub is off-center and runout is a measure of deviation of the rim from a true circle.

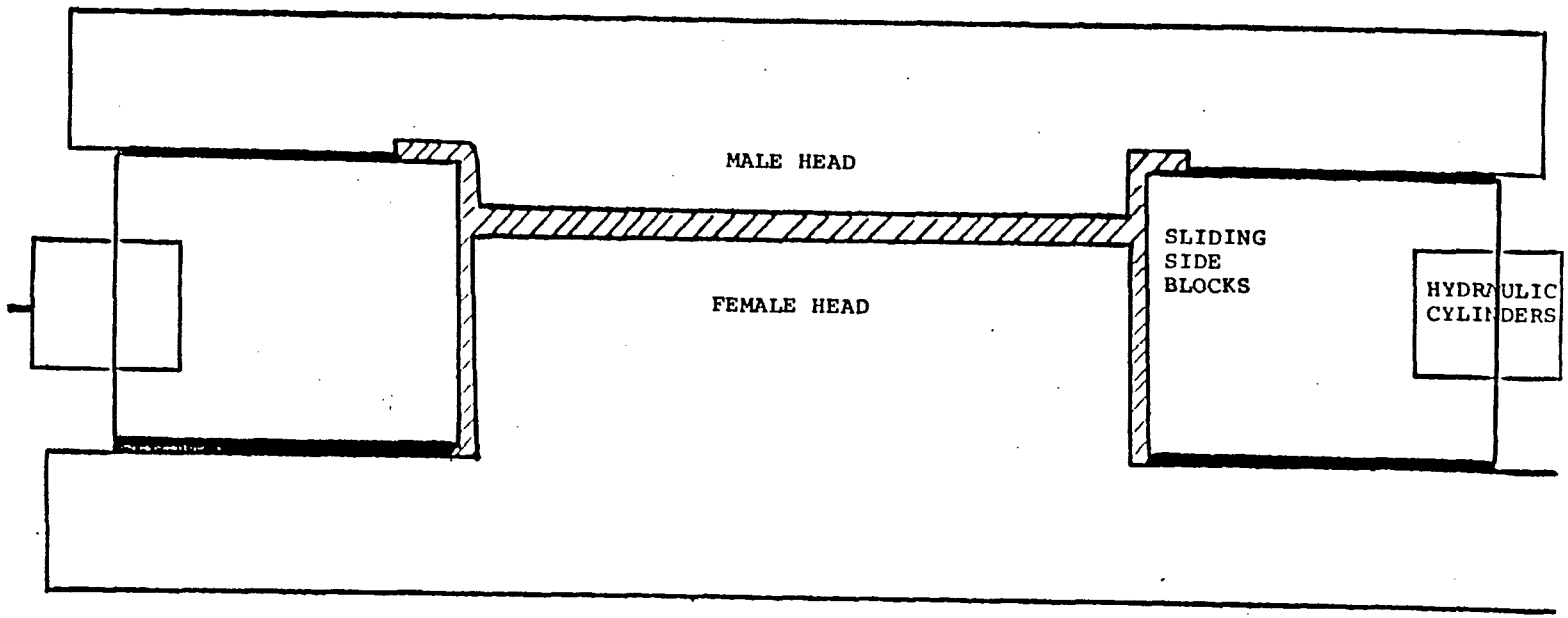

Figure 44 Schematic of Wheel Mold

8.3.1 To minimize eccentricity and runout during the manufacturing process, two important parameters must be precisely controlled. These parameters are:

8.3.1.1 Blanking of the composite laminates

8.3.1.2 Molding procedures while the composite is in the mold.

8.4 Composite Laminate Blanking

The continuous glass laminates were stacked with the required fiber orientation (as dictated by wheel design) and cut using steel templates. This ensured proper fiber orientation, weight, and size of the preform.

8.4.1 The discontinuous glass reinforced sheet was blanked using different steel templates, which are smaller than the templates for the continuous fiber laminates. The small blanks of randomly oriented glass laminates flow during the molding cycle, thus eliminating air entrapment in the molded wheels. Again the preform blank was cut to closely controlled weight and dimensional specifications.

8.4.2 The use of steel templates to cut the blanks from continuous unidirectional glass compound sheet ensured size consistency of each blank. Furthermore, each composite charge was weighed before placing it in the mold. The weight tolerance of the laminated composite blank was controlled to ensure specified weight tolerance of the wheel before molding.

8.4.3 In addition to the above procedures, use of steel molds maintained weight control of the finished product by preventing material from escaping during the molding process.

8.5 Weight Control

8.5.1 The following steps were adopted to control the weight of the plastic wheel:

8.5.1.1 The continuous unidirectional glass composite was supplied as uncured unidirectional prepreg on a roll with the proper width up to 48" (1219 mm) wide.

8.5.1.2 Each ply was cut in a circular preform shape and stacked to form the continuous fiber laminates. The plies were stacked so as to maintain the fiber orientation required by the design.

8.5.1.3 The chopped glass molding compound was supplied in a thick sheet form with close tolerance in terms of weight per unit area.

8.5.1.4 A special steel template was used to cut the chopped glass composite sheet to the proper configuration. The blank was then flattened on a press to level any irregularities that may exist.

8.5.1.5 The continuous glass fiber laminate was then laminated to the discontinuous glass blank. The air between the plies was evacuated using a vacuum pump. This resulted in a charge ready for molding.

8.6 Wheel Molding

8.6.1 After the blank was cut and ready for placement in the mold, the following procedures were adopted:

8.6.1.1 The blank was placed on the bottom half of the heated mold, which is installed in a hydraulic press.

8.6.1.2 The mold is closed by the press hydraulic system.

8.6.1.3 The molding parameters were 1000 psi (6.895 MPa) pressure, 300 degrees F (148.9 deg.C) mold temperature, and a 20 minute cure cycle. The specified pressure is 800 to 1000 psi (5.516 to 6.895 MPa), while the specified temperature is 280 to 300 degrees F (137.8 to 148.9 deg. C). The upper limits of these parameters were used to assure quality wheel moldings.

8.6.1.4 At the end of the cycle, the press pressure was released and the mold was opened.

8.6.1.5 The cured composite wheel was ejected from the mold.

8.6.1.6 Each wheel was trimmed and inspected.

8.6.1.7 The mold surfaces were cleaned and sprayed with a mold release compound. (This is done to prevent the part from sticking to the mold).

8.6.2 A photograph of the compression molding press used in this process is shown in Figure 45.

8.7 Discussion of the Manufacturing Process

8.7.1 The first attempts at composite wheel fabrication utilized an all continuous glass compound oriented in the design directions (radial and circumferential). This type of material, however, did not produce consistent molded wheels. All that was learned in this phase was the charge weight was approximately 44 pounds(19.96 Kg). After several trials, a final charge pattern was developed.

8.7.2 Composite wheels were manufactured using two different glass orientations. The first group of wheels were molded using an equal amount of continuous and discontinuous glass reinforcement (50% XMC, 50% HMC). The second group was molded using a high percentage of continuous glass (XMC type material) in a circumferential and in a radial direction.

8.7.3 Preliminary Inspection of Completed Composite Wheel Assembly.

Upon completion of manufacturing, a tire, tube, and flap were mounted on the plastic wheel and lock ring. The tires were inflated to 90 psi (621 KPa). The air pressure was checked periodically over several months and no loss in air pressure was noted. The lock ring also remained in place. This completed the manufacturing process. No C-scan was performed.

9.0 COMPOSITE WHEEL TESTING

9.1 Mounting and Demounting

One of the considerations in the use of composite wheels was mounting and demounting the tire, tube and flap to and from the wheel. Using standard steel tools, the tire with tube and flap was mounted to the composite wheel and demounted. The tire was inflated to approximately 95 psi (665 KPa) and held for 30 minutes. The maximum inflation pressure achieved was 105 psi (724 KPa). Mounting and demounting were repeated ten (10) times. No detrimental effects on the wheel were observed. Figure 46 is a photograph of the tire mounted on the wheel, while Figure 47 illustrates some wear on the lock ring after nine demountings.

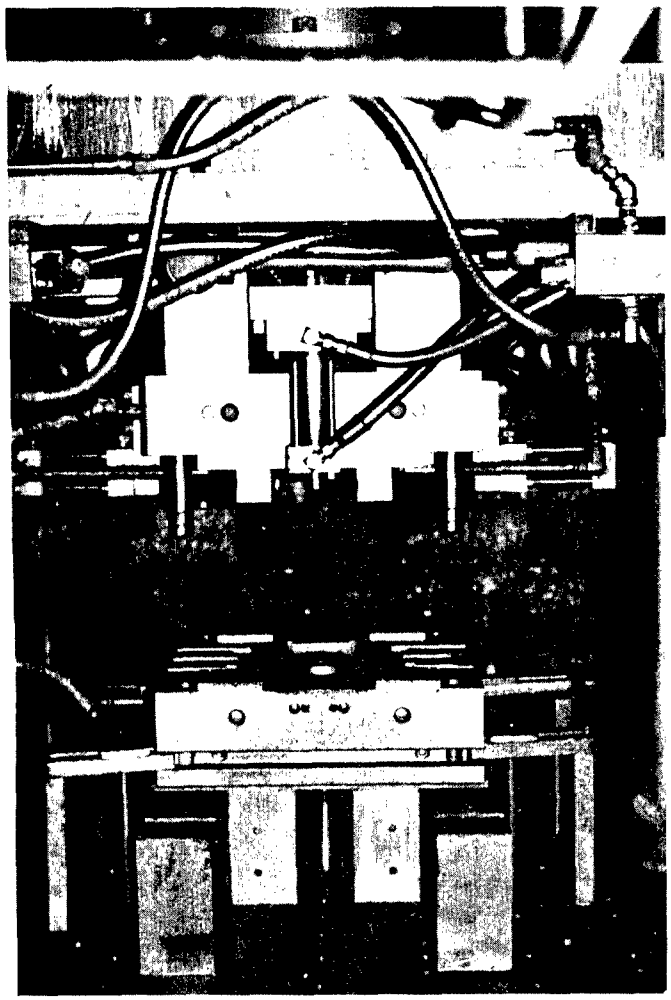

Figure 45 500 Ton Hydraulic Press to be Used in Manufacturing Leaf Springs and Wheel Assemblies

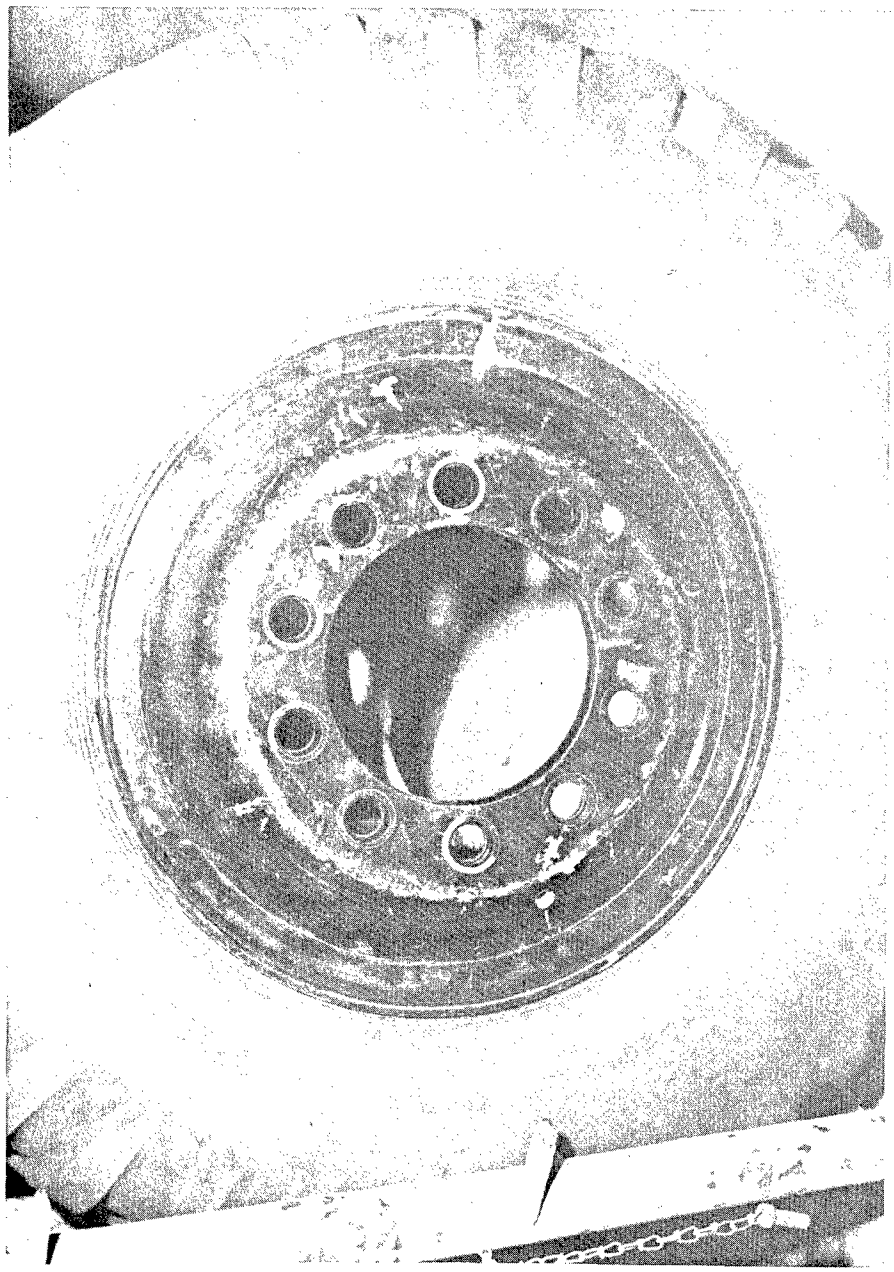

Figure 46 Wheel with Tire Mounted

Figure 47 Close-up of Mounted Tire Showing Wear on Lock Ring after nine demountings

9.2 Testing at Budd Wheel

Composite Wheels previously described were subjected to testing at the facilities of the Budd Company located in Detroit, Michigan. In order to determine whether these wheels would perform as well as the basic steel wheel, they were subjected to the Dynamic Radial Fatigue Test in accordance with the procedure described in SAE J267A. The first test conducted was the dynamic cornering fatigue test. In this test a selected axial load was applied to the hub and lug bolt while spinning the wheel rim at a constant rate. The axial load was applied to provide a bending moment to simulate the loading condition encountered during vehicle cornering.

The wheel was mounted to a rotating mounting plate to which the rim flange was securely clamped. The composite wheel was fastened to the test hub by bolts and ten flat-faced nuts with a bearing area 1 11/16 inches (42.86 mm) in diameter. The wheel nuts were tightened to the hub with a torque equal to 450 ft-lbs. (610 Meter-Newton). The test hub was bolted to a horizontal load shaft as shown in Figure 48.

9.2.1 Load vs. deflection was determined for wheel #1 and wheel #2.

Data is shown in Tables 3 and 4.

9.2.2 The clamped composite wheel without any applied load was within the specified eccentricity of 0.010" (0.254 mm) normal to the point of loading. The applied load was maintained at a nominal angle of 40 degrees from a plane through the center of the rim. The test loads were applied in increments of 1,000 lbs. (4448 Newtons) up to the maximum capacity of the testing machine (14,000 lbs., or 62,275 Newtons). The applied load and the deflection of the shaft were monitered and measured after each load increment. The maximum static deflection of the shaft for wheel #1 reached 0.237 inch (6.02 mm) at 14,000 lbs. The load was then decreased gradually back to 0 and the deflection of the shaft was again monitored. The static test Data of this wheel is shown in Table 3. No permanent deformation or deflection was noticed during the test.

9.2.3 The composite wheel was then subjected to the maximum load of 14,000 lbs., and the cornering fatigue test started. The load was applied with a moment arm of 39", thus, a bending moment of 45,500 ft.-lbs. (61690 meter- Newton) was applied

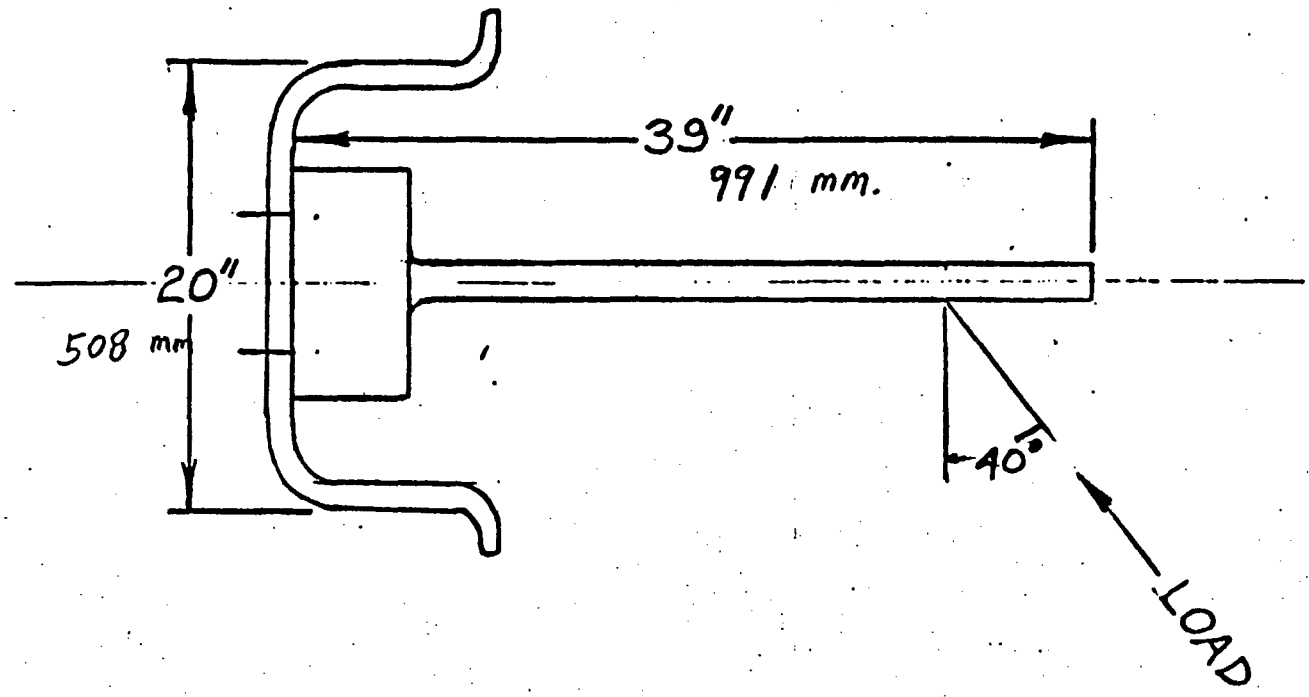

Figure 48 Composite Wheel Mounting and Direction of Load Application.

TABLE #3

Static load-deflection Readings of Composite Wheel #1

LOAD APPLIED POUNDS	DEFLECTION UP INCHES	DEFLECTION DOWN INCHES
700	Zeroed out	0.018
1700	0.021-0.018-0.019	*
2700	0.038-0.033-0.035	
3700	0.067-0.06-0.055	
4700	0.087-0.084-0.087	
5700	0.104-0.100 First Jump	
6700	0.119-0.119 Started over	
7700	0.136-0.136	
8700	0.151-0.156	
9700	0.167-0.175	
10700	0.181-0.193	
11700	0.196-0.212	
12700	0.212 Second Jump	
13700	0.230 Started over	
14700	0.237	

14000 After approximetely 2 minutes 0.244

*No readings were taken going down except for the one at the 700.

TABLE #4

Static load-deflection Readings of Composite Wheel #2

LOAD APPLIED POUNDS	DEFLECTION UP INCHES	DEFLECTION DOWN INCHES
700	Zeroed Out	0.004
1700	0.025	0.036
2700	0.041	0.075
3700	0.055	0.094
4700	0.068	0.108
5700	0.080	0.120
6700	0.108	0.134
7700	0.125	0.142
8700	0.135	0.155
9700	0.146	0.164
10700	0.158	0.174
11700	0.170	0.184
12700	0.180	0.193
13700	0.194	0.201
14000	0.206	
14000 After approximately 2 minutes	0.210	

during the entire test. The test continued until a measured deflection of 0.020 inches (0.508 mm) was detected. This deflection occurred after 340 revolutions. The testing machine automatically stopped. The setting was redjusted to allow axle deflection up to 0.060 inches (1.524 mm) and the test started again. After several revolutions, this deflection was reached and the testing machine automatically stopped. Although there was no visible failure of the composite wheel, the capability of the machine could not allow any higher deflection while maintaining the maximum bending moment on the wheel.

Thus, the test was terminated. The plastic wheel was dismounted from the machine and examined.

Details of the composite wheel mounting and testing are shown in Figures 49 to 58.

9.2.4.1 Examination of the composite wheel, revealed several long cracks extending between the mounting bushings. Other cracks were also evident through the disc area of the wheel.

9.2.5 The following observations were reported:

9.2.5.1 The wheel had moderate cracks on the inner and outer surfaces, but none appeared to penetrate the complete disc section.

9.2.5.2 The initial torque on the 10 wheel nuts dropped by an average of 110 ft.-lbs.(149 meter-Newtons) per nut. This condition could have had a significant effect on the deflection displayed during the test.

9.3 FATIGUE TEST - COMPOSITE WHEEL #2

The exact procedures as outlined above were followed in testing this wheel. The wheel was attached to the wheel hub by means of 10 ball seating nuts, the same type as currently used on steel wheels. Each nut was torqued at 350 ft.-lbs.(475 meter-Newton). The test was conducted in the same manner, according to SAE J267A.

9.3.1 The wheel was subjected to the 14,000 lbs. axial load and rotated until a deflection of .020" was detected. This deflection occurred after 1,440 revolutions. Upon increasing the allowable deflection on the machine to 0.060 inch, the wheel testing continued. The 3,200 test cycles were accumulated when the 0.060 inch deflection limit was reached. At this point, the test was discontinued. The wheel was dismounted and examined for visible cracks or evidence of failure.

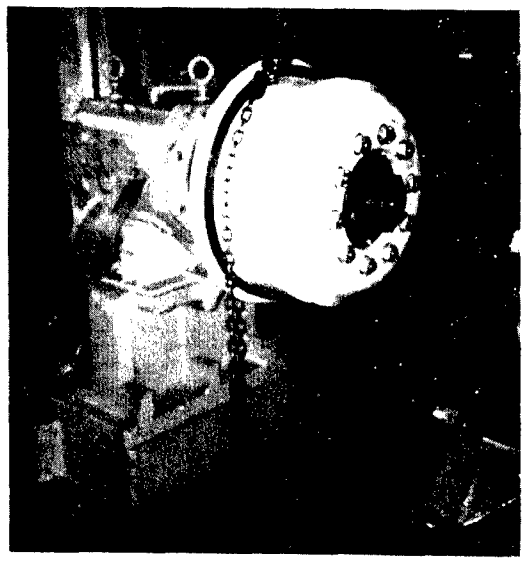

Composite Wheel Set Up for Tightening
Wheel Nuts to Fixture Studs (Wheel #3).
Figure 49

Instrumentation of Test Fixture to Measure
Axle Deflection Under Static Loads (Wheel #3)
Figure 50

Composite Wheel During Cornering Fatigue
Test Wheel #3).
Figure 51

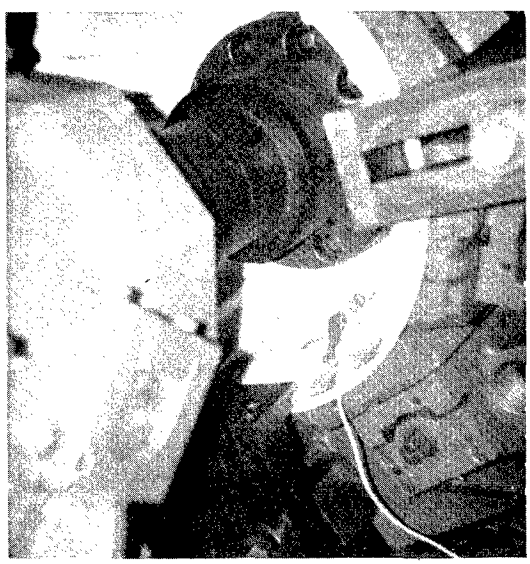

Non-Destructive Testing of Composite Wheel Using
accoustical Emmission methods (Wheel #1)
Figure 52

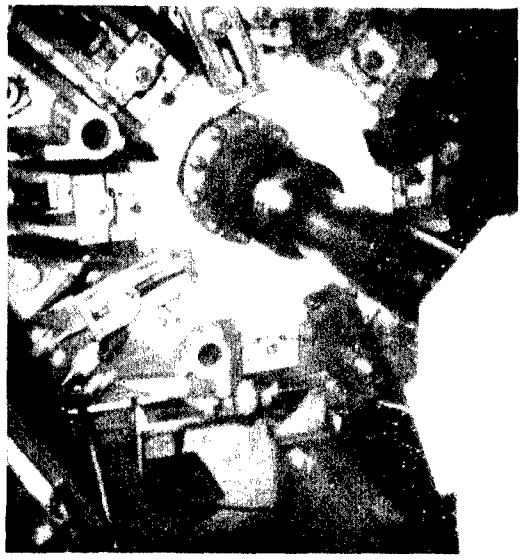

Mounting of Composite Wheel with Steel Ring
Using Conventional Clamps (Wheel #1)
Figure 53

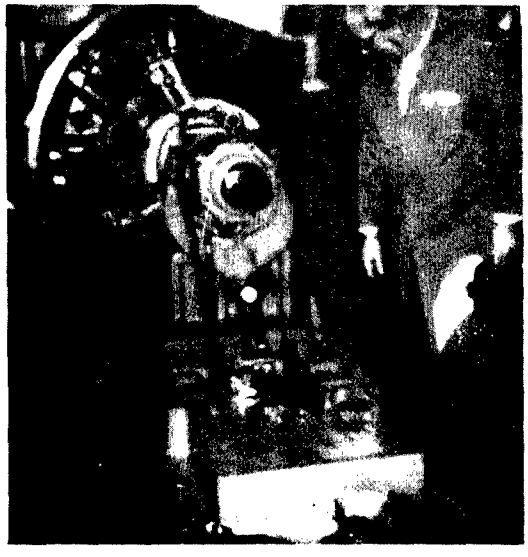

Set-Up of Stationary Deflection Test and
Instrumentation of Plastic Wheel for measuring
Torque versus Deflection (Wheel #1)
Figure 54

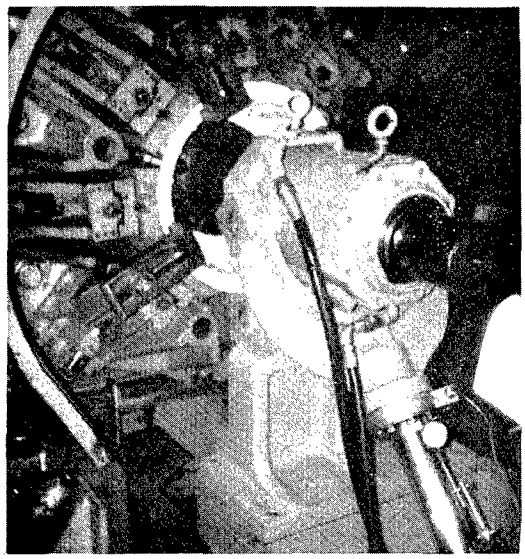

Close-Up of the Composite Wheel Mounted to the Hub and Axle of Cornering Fatigue Testing Machine.

Figure 55

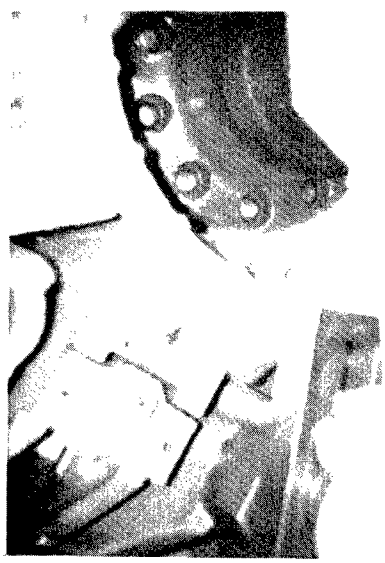

Composite Wheel During Fatigue Test, Adhesive Bond between Steel Ring and Composite Wheel Disc Shearing Out.

Figure 56

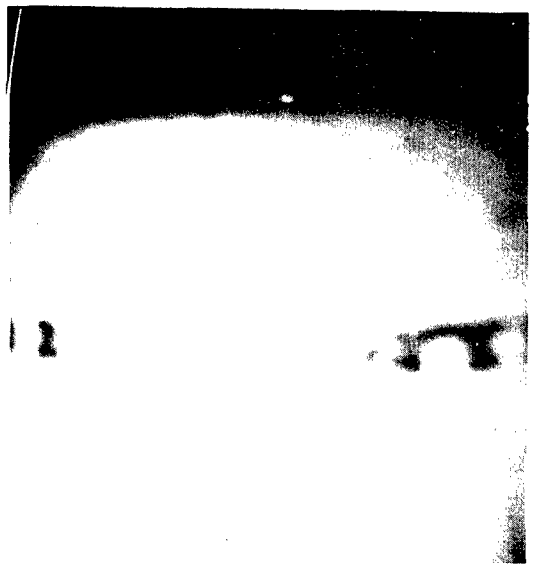

Steel Ring Seperated from Composite Wheel Disc due to Adhesive Failure after 3,400 Fatigue Cycle under Maximum Loads.
Figure 57

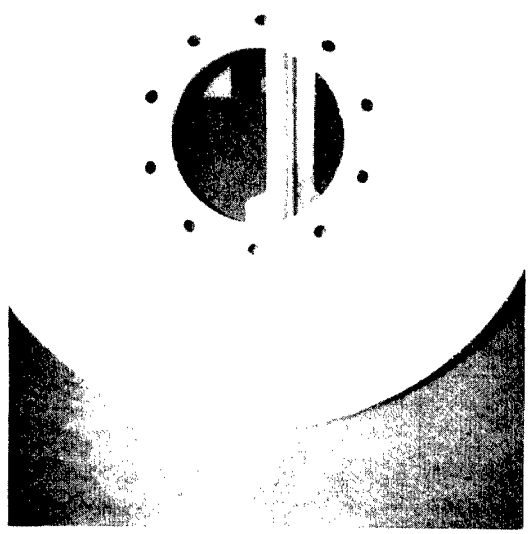

Close-Up of Adhesive Resin Separation after Completion of the Fatigue Test.
Figure 58

9.3.2 The following observations were reported:

9.3.2.1 The wheel had small cracks on the inner and outer surfaces of the disc. The size of these cracks was smaller than those experienced in the first wheel. None of the cracks penetrated through the disc section.

9.3.2.2 There was a significant drop in the initially applied torque on the attaching nuts. This drop in torque allowed the excessive deflection of the disc and the consequent need to stop the test.

9.3.3 It appears that the mounting system adapted for the second wheel exhibited more rigidity, and reduced cracking and deformation of this wheel. Wheels with inserted bushings exhibited a significant number of cracks that propagated throughout the section of the wheel disc. Further testing was conducted modifying the type of steel reinforcement attached to the wheel hub. Spring steel discs with a thickness of .020" or slightly thicker was fabricated and attached to the composite wheels.

9.3.4 It is important to note that the design load of this composite wheel was based on 5,200 pounds (2359 Kg or 23131 Newtons) load. A safety factor of about 2.7 was applied resulting in an applied load of 14,000 pounds (6350 Kg or 62275 Newton) during the initial phase of this testing. The recommended practice of the SAE test procedures requires a factor of 1.9. This will require a maximum test load of 9,880 pounds (43948 Newtons). These modifications were adopted during the next phase of testing.

9.4 Endurance Test (MIL SPEC T-12459D)

9.4.1 Upon completion of dynamic radial fatigue testing, further dynamic testing was performed on the National Bureau of Standards Test Machine to determine whether the wheels could perform in the indoor endurance test of Military Specifications MIL-T-12459D dated 31 December 1979. The tires used were 1100 X 20 NDCC 12 ply. Four wheels were prepared. The tires were inflated to 85 psi (586 KPa) cold. The test setup is as shown in Figure 59.

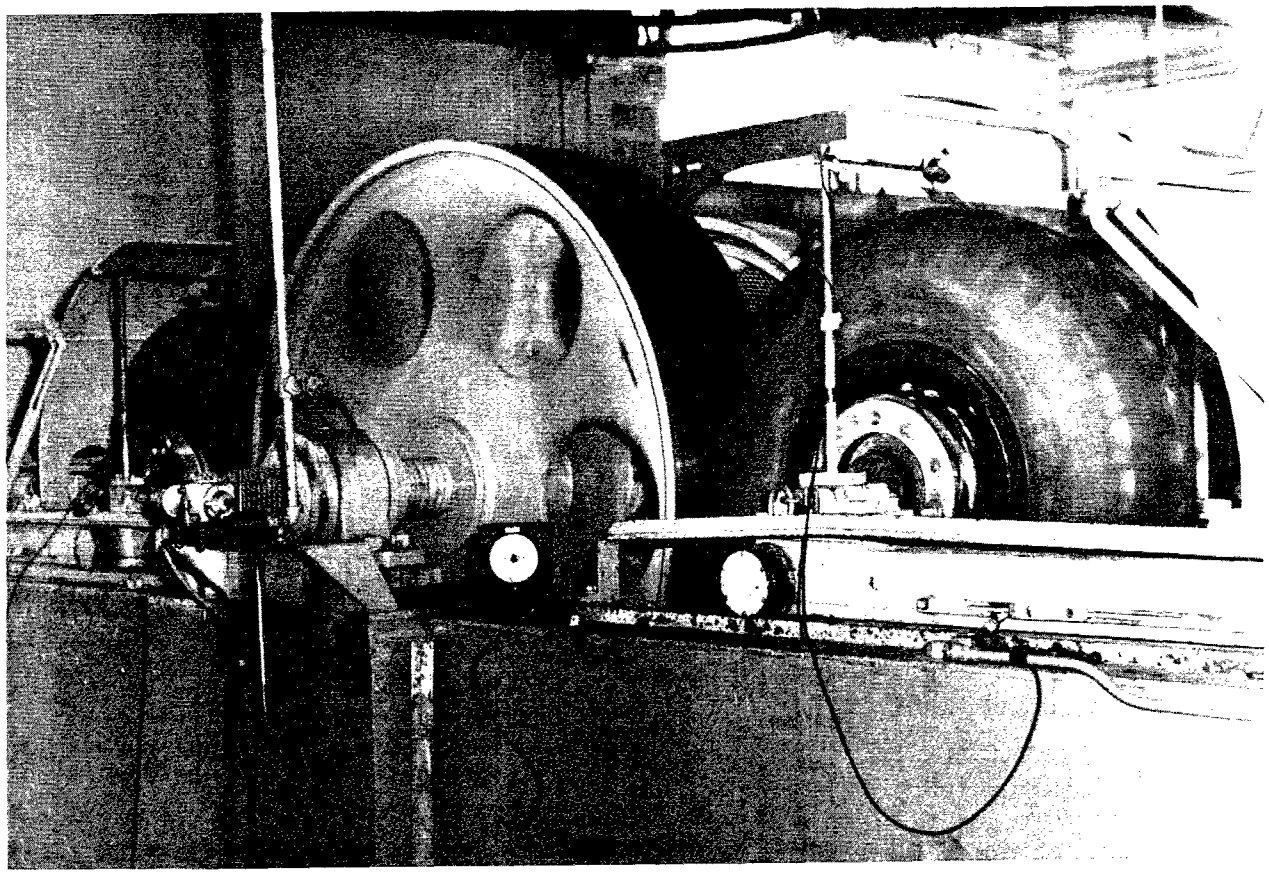

Figure 59 Test Set-up for Indoor Endurance Test.

The test requirements were as follows:

Wheel speed 30 MPH (48.3 Km/hr)

Wheel Load		Time
Pounds	Newtons	Hours
3645	25.131	7
4690	32.336	16
6160	42.472	24

Test Temperature = 99 degrees F (37.2 deg.C)

Wheel to axle bolts were tightened to 100 ft-lbs. (136 meter-Newton).

Metal rings were used on both sides of the composite wheel for mounting purposes.

9.4.2 Test results were as follows:

9.4.2.1 Tire air pressure climbed and held at 94 psi.(648 KPa)

9.4.2.2 The wheel surface temperature increased to 115 degrees F (46.1 deg C) and 130 degrees F (54.4 deg C) was recorded between tire and wheel via a gap in the side ring.

9.4.2.3 Composite wheel sample A endured for 11 hours, then disintegrated into several pieces allowing the tire bead to slip over the wheel, causing the tube to be punctured. The machine automatically disengaged at this point. (see Figures 61 thru 64).

9.4.3 Another composite wheel was tested using the same procedures outlined above. This wheel (sample B) endured the load for 21 hours, 30 minutes, then was shut down manually. The test was stopped due to several cracks in the wheel surface (see figure 60).

9.4.4 Sample #7 ran 7 hours at 3645 lb. (70% single tire load), and 4 hours, 42 minutes at 4690 lb. (90% single tire load). At this time the wheel lock ring blew apart, shattered into several pieces and punctured the inner tube. The test was then halted.

9.4.5 Sample #4 ran 7 hours at 3645 lbs. 16 hours at 4690 lbs., and 8 hours at 5330 lbs (110% single tire load). The test was then stopped because of several cracks in the wheel and lock ring, which created a serious safety hazard. All testing for samples #4 and #7 was conducted at 30 MPH.

Figure 60 Sample B, after test was Stopped Due to Fatal Cracking.

On samples 4 and 7, locking rings from samples A and B were used.

Upon stopping the tests, the wheels were examined. Many cracks were noted. Both of the wheels cracked and broke out at the lip. See figures 61 and 64 for the cracking.

9.4.5.1 The failed locking ring was sectioned and examined. (Figures 65 and 66) The failure occurred under the tire bead where the fracture was completely through the cross section of the ring. This caused a section to break out, with the remaining section puncturing the inner tube. Lack of adhesion between the resin system and the directional fibers appears to be the cause of the failure. In addition, the sectioned ring reveals some minor porosity at the interface between the continous and discontinuous glass compound.

9.4.6 The tested wheels were examined using the following techniques:

9.4.6.1 Visual examination - inspection, using intense light and magnifying glasses.

9.4.6.2 X-ray examination

9.4.6.3 Photographic inspection of sectioned wheels

9.4.7 These inspections revealed the following:

9.4.7.1 Some cracks were observed in the tested wheels.

9.4.7.2 No discontinuity or major separation in the resin matrix could be detected.

9.4.7.3 Some voids were scattered throughout the wheel cross section, especially in the hub area.(Figure 67)

9.4.7.4 Some of the continuous reinforcing fibers were kinked and wavy. (This was attributed to the design of the mold). This phenomena called "marcelling", was a major cause of the failure of the composite wheels during testing.

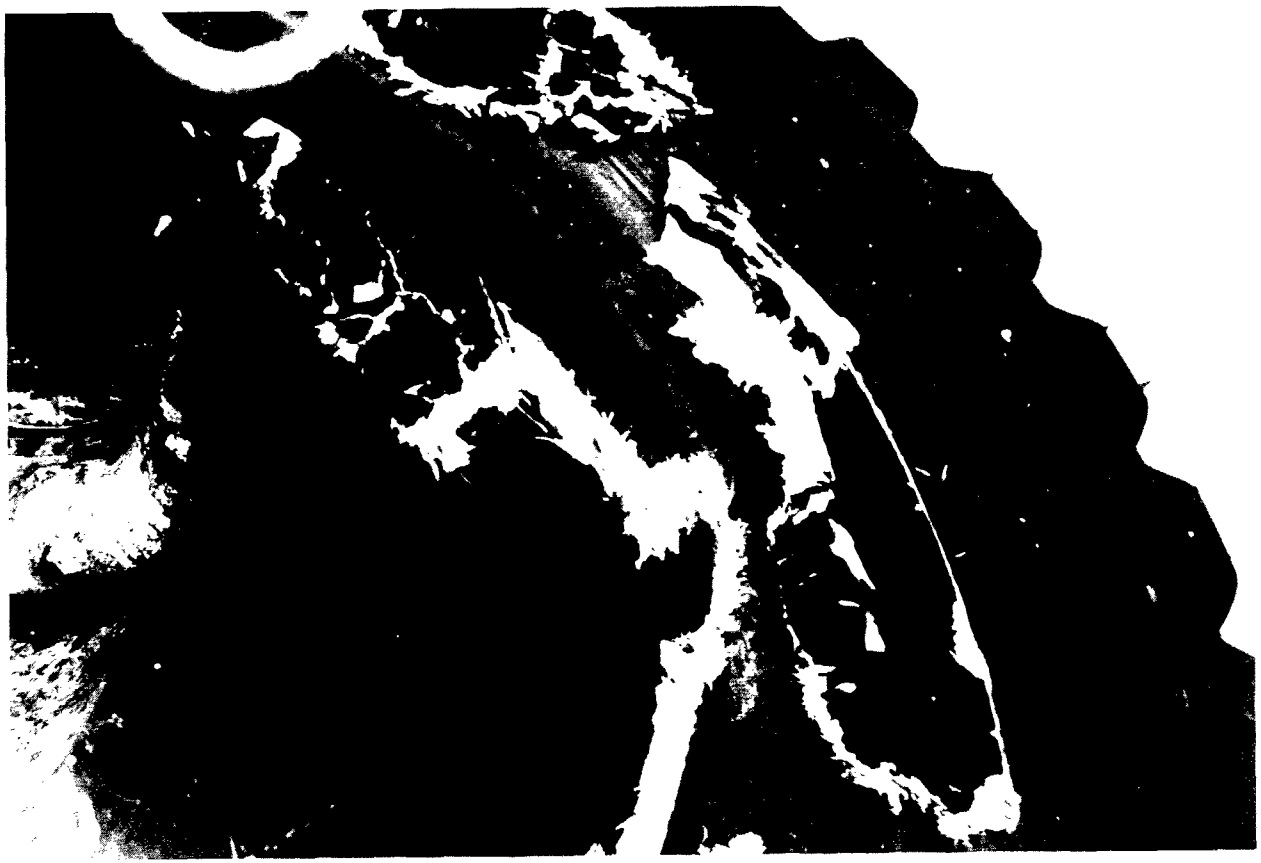

Figure 61 Sample A, after Failure Showing Location of Pieces Broken Off.

Figure 62 Sample A, after Failure Showing Damaged Section.

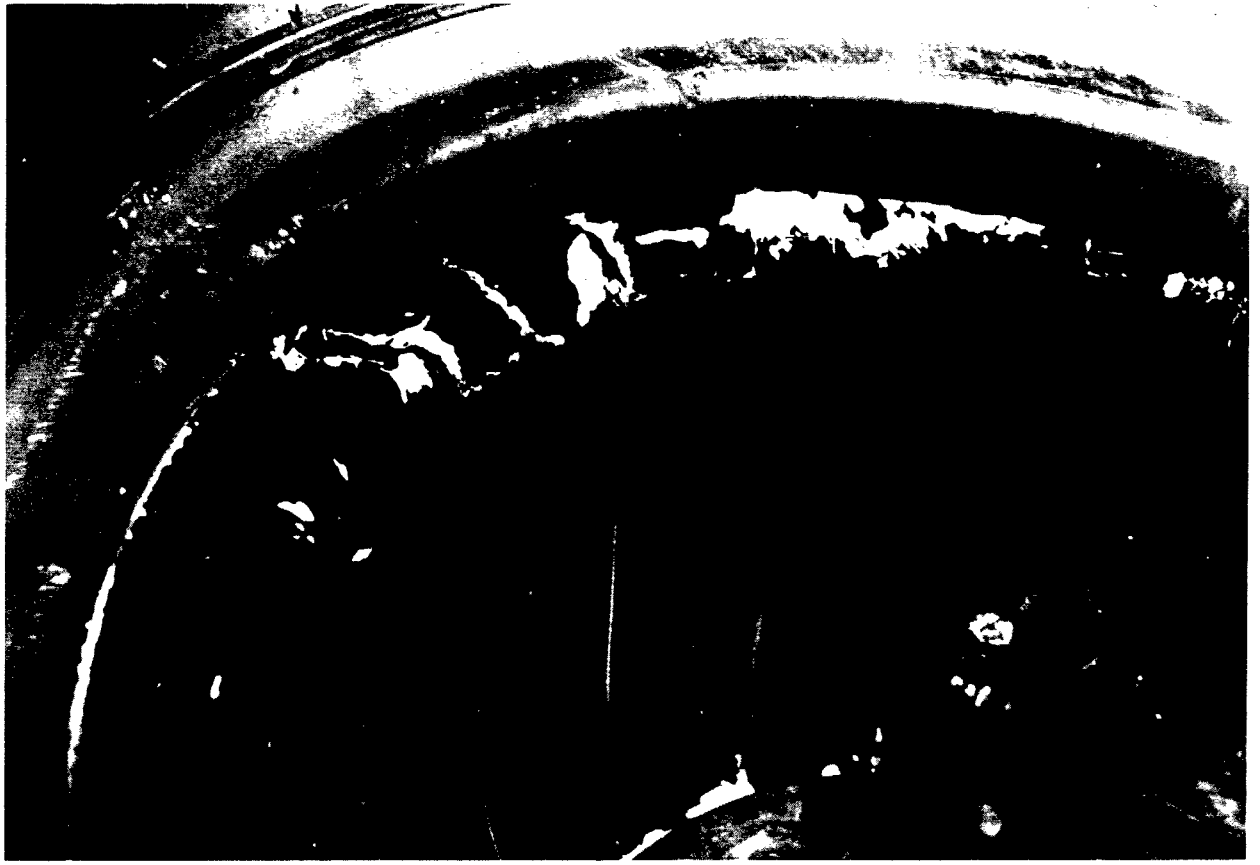

Figure 63 Sample A, after Failure Showing Section where Tire Started to Separate from Composite Wheel.

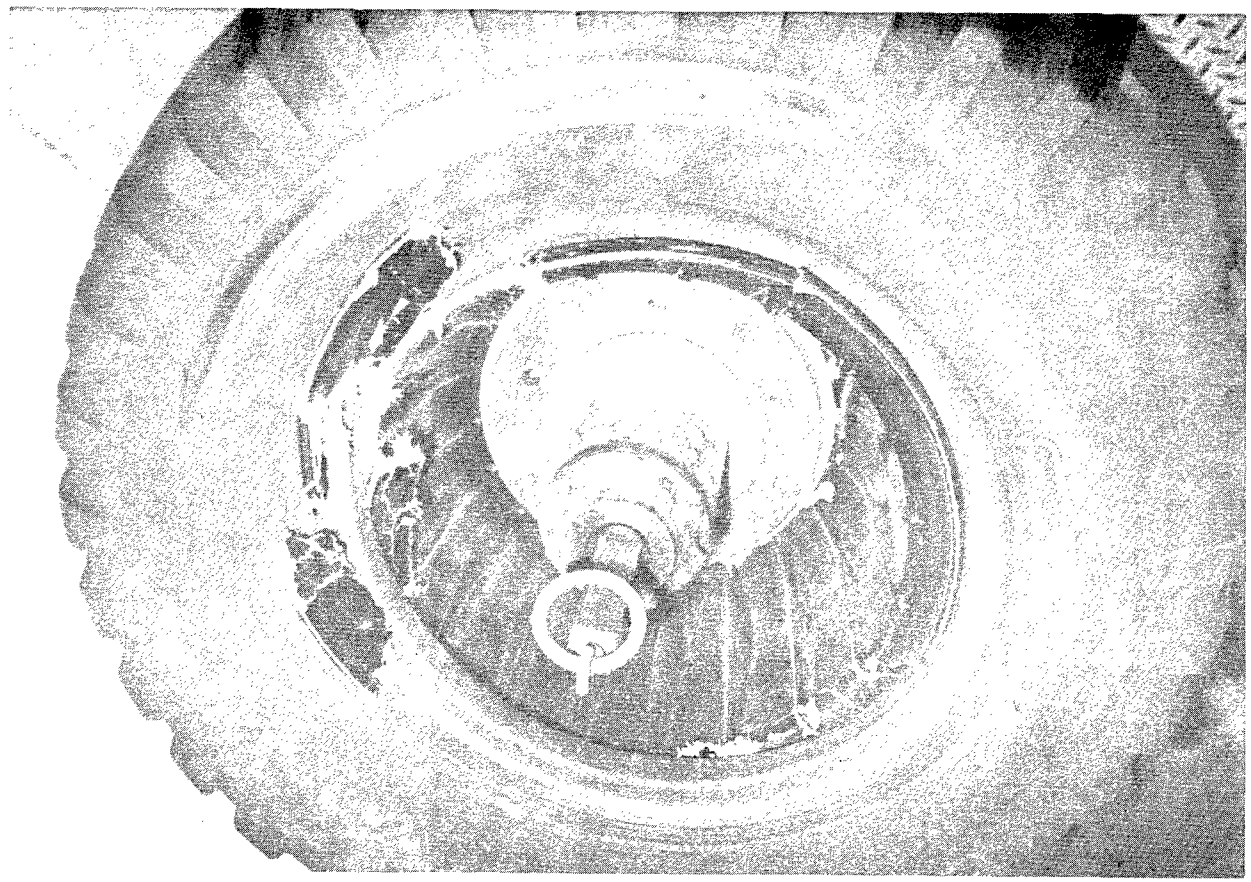

Figure 64 Sample A Failure Showing Overall View of Tire and Rim Assembly.

Figure 65 Locking Ring after Failure

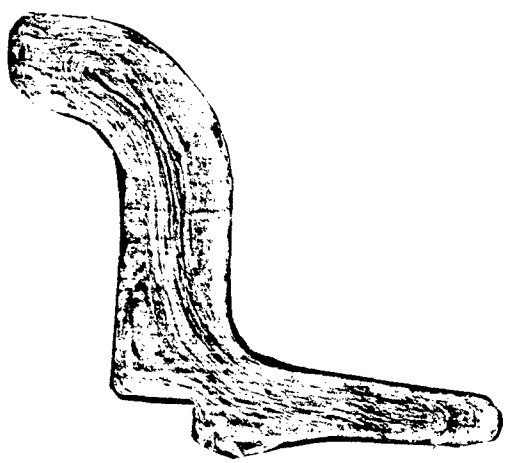

Figure 66 Cross-Section of Locking Ring

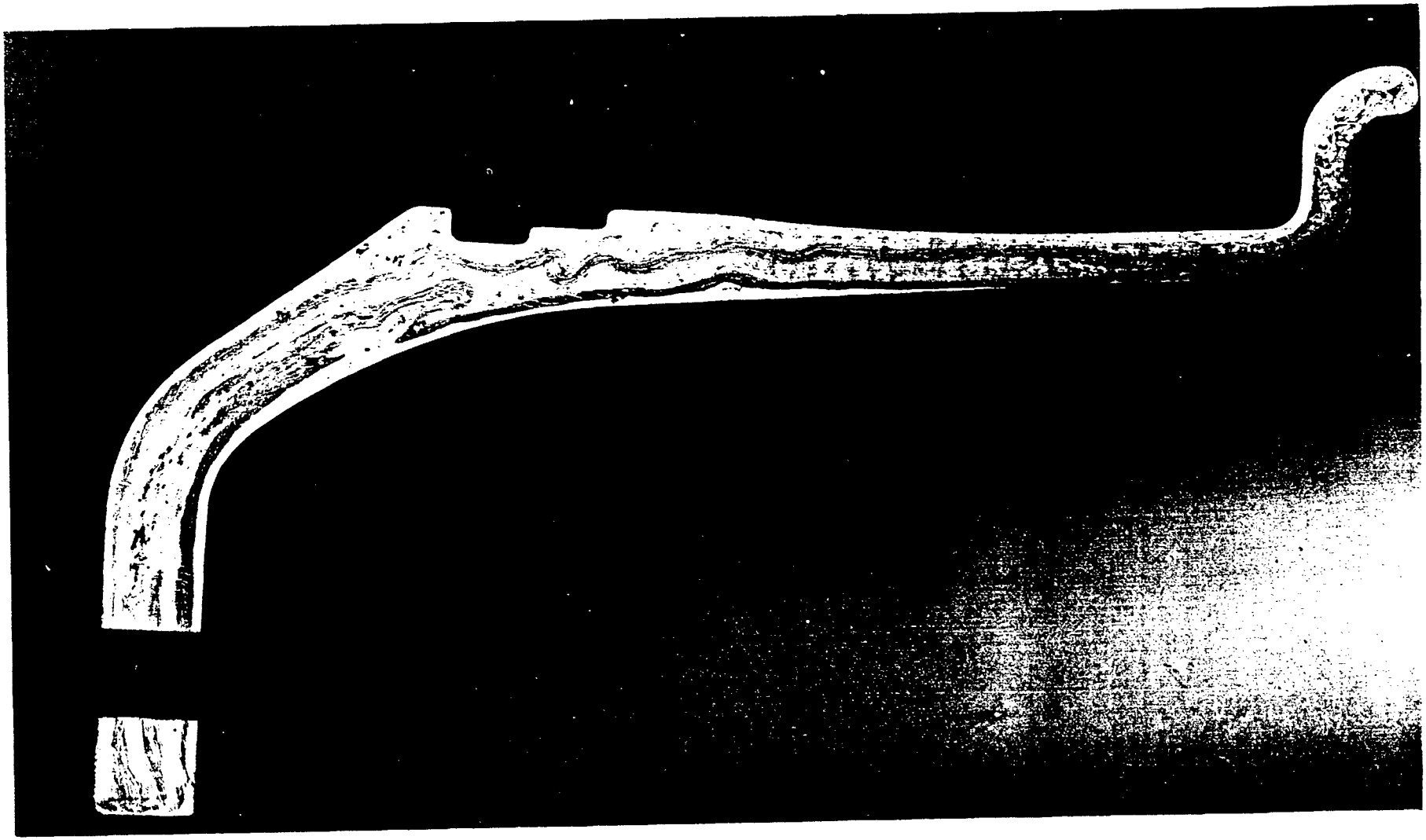

Figure 67 Cross-Section of Wheel

10.0 CONCLUSIONS

10.1. Wheels can be made from structural composites.

10.2. Manufacturing procedures for the wheel must be revised to prevent marcelling.

10.3. The resin system requires improvement to prevent delamination in the spinning load.

10.4. The design criteria are adequate.

11.0 RECOMMENDATIONS

11.1 The method of manufacturing must be improved or be restructured to prevent marcelling.

11.2 More testing must be done prior to quantity production.

11.3 Non-destructive techniques should be applied throughout the manufacturing process.

Distribution List

	Copies
DEFENSE TECHNICAL INFORMATION CENTER ATTN: DTIC-CTA Cameron Station Alexandria, VA 22314	12
Commander US ARMY MATERIAL DEVELOPMENT AND READINESS COMMAND ATTN: DRCMT 5001 Eisenhower Avenue Alexandria, VA 22333	1
Director US ARMY MATERIALS AND MECHANICS RESEARCH CENTER ATTN: DRXMR-RC Watertown, MA 02172	2
PLASTEC Picatinny Arsenal Dover, NJ 07801	1
Commander US ARMY TACOM ATTN: DRSTA-TSL DRSTA-R DRSTA-NS DRSTA-RCKM DRSTA-G DRSTA-RSC Warren, MI 48090	 3 1 1 1 1 2
HQ, DEPT OF THE ARMY Deputy Chief of Staff for Research, Development and Acquisition ATTN: DAMA-ARZ-E Washington, DC 20310	1
EXXON ENTERPRISES MATERIALS DIVISION PO Drawer H Greer, SC 29651	2
EWALD ASSOC, INC 19450 Fitzpatrick Detroit, MI 48276	1

	Copies
CIBA-GEIGY Riggs Engineering Dept 8245 A Ramson Road San Diego, CA 92111	1
UNIVERSITY OF WYOMING ATTN: D.F. Adams Rm 259, College of Engr Laramie, WY 82071	1
NAVAL MATERIAL COMMAND Code (MAT0424) Washington, DC 20360	1